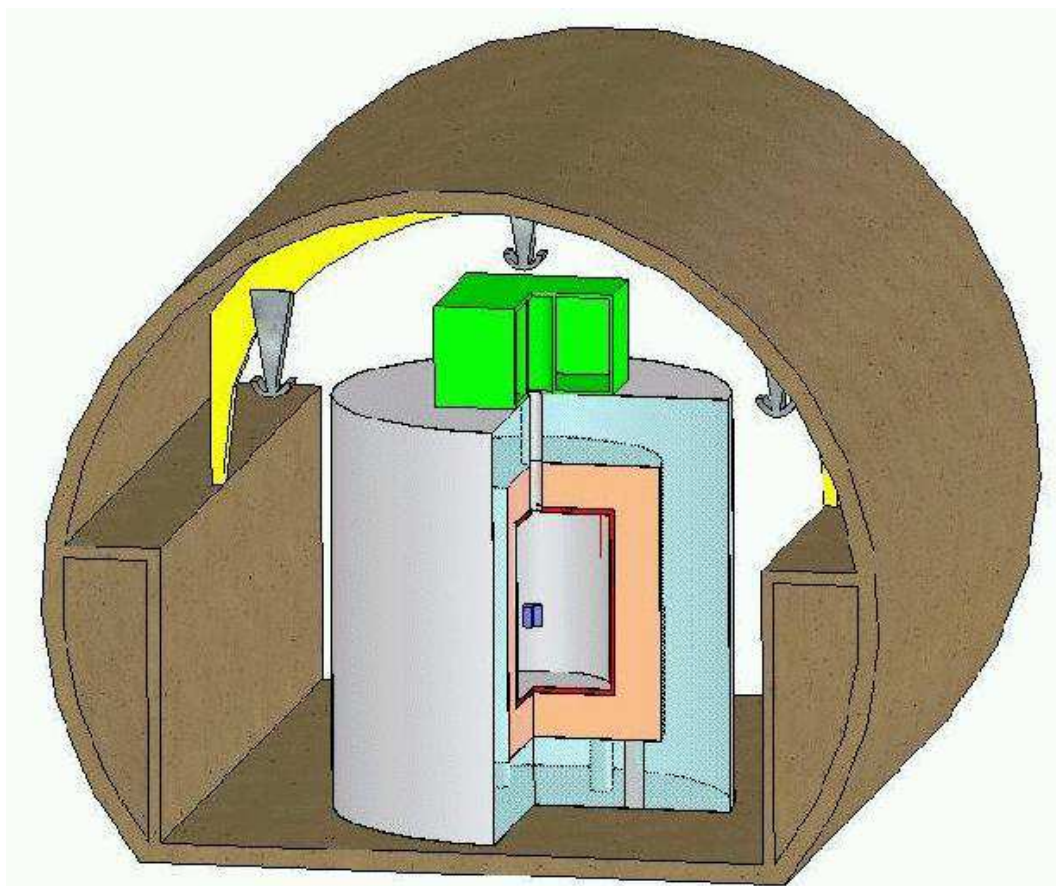


# A New $^{76}\text{Ge}$ Double Beta Decay Experiment at LNGS

arXiv:hep-ex/0404039v1 29 Apr 2004



## Letter of Intent

16 March 2004

# A New $^{76}\text{Ge}$ Double Beta Decay Experiment at LNGS

I. Abt<sup>i</sup>, M. Altmann<sup>i</sup>, A. Bakalyarov<sup>h</sup>, I. Barabanov<sup>f</sup>, C. Bauer<sup>c</sup>, E. Bellotti<sup>e</sup>,  
S.T. Belyaev<sup>h</sup>, L. Bezrukov<sup>f</sup>, V. Brudanin<sup>b</sup>, C. Büttner<sup>i</sup>, V.P. Bolotsky<sup>g</sup>, A. Caldwell<sup>i</sup>,  
C. Cattadori<sup>a,e</sup>, H. Clement<sup>j</sup>, A. Di Vacri<sup>a</sup>, J. Eberth<sup>d</sup>, V. Egorov<sup>b</sup>, G. Grigoriev<sup>h</sup>,  
V. Gurentsov<sup>f</sup>, K. Gusev<sup>b</sup>, W. Hampel<sup>c</sup>, G. Heusser<sup>c</sup>, W. Hofmann<sup>c</sup>, J. Jochum<sup>j</sup>,  
M. Junker<sup>a</sup>, J. Kiko<sup>c</sup>, I.V. Kirpichnikov<sup>g</sup>, A. Klimenko<sup>b,f</sup>, K.T. Knöpfle<sup>c</sup>,  
V.N. Kornoukhov<sup>g</sup>, M. Laubenstein<sup>a</sup>, V. Lebedev<sup>h</sup>, X. Liu<sup>i</sup>, I. Nemchenok<sup>b</sup>,  
L. Pandola<sup>a</sup>, V. Sandukovsky<sup>b</sup>, S. Schönert<sup>c</sup>, S. Scholl<sup>j</sup>, B. Schwingenheuer<sup>c</sup>,  
H. Simgen<sup>c</sup>, A. Smolnikov<sup>b,f</sup>, A. Tikhomirov<sup>h</sup>, A.A. Vasenko<sup>g</sup>, S. Vasiliev<sup>b,f</sup>,  
D. Weißhaar<sup>d</sup>, E. Yanovich<sup>f</sup>, J. Yurkowski<sup>b</sup>, S. Zhukov<sup>h</sup>, G. Zuzel<sup>d</sup>

<sup>a</sup> INFN Laboratori Nazionali del Gran Sasso, Assergi, Italy

<sup>b</sup> Joint Institute for Nuclear Research, Dubna, Russia

<sup>c</sup> Max-Planck-Institut für Kernphysik, Heidelberg, Germany

<sup>d</sup> Institut für Kernphysik, Universität Köln, Germany

<sup>e</sup> Università di Milano Bicocca e INFN Milano, Milano, Italy

<sup>f</sup> Institute for Nuclear Research of the Russian Academy of Sciences, Moscow, Russia

<sup>g</sup> Institute for Theoretical and Experimental Physics, Moscow, Russia

<sup>h</sup> Russian Research Centre Kurchatov Institute, Moscow, Russia

<sup>i</sup> Max-Planck-Institut für Physik, München, Germany

<sup>j</sup> Physikalisches Institut, Universität Tübingen, Germany

## Contact Persons:

W. Hofmann

(*Werner.Hofmann@mpi-hd.mpg.de*)

S. Schönert,

(*Stefan.Schoenert@mpi-hd.mpg.de*)

# Contents

<b>1</b>	<b>Overview and executive summary</b>	<b>5</b>
<b>2</b>	<b>Introduction and experimental overview</b>	<b>9</b>
2.1	Introduction . . . . .	9
2.2	Past and present experiments . . . . .	11
2.3	Proposed and suggested future experiments . . . . .	11
<b>3</b>	<b>Design considerations:background sources and discrimination methods</b>	<b>14</b>
3.1	Background sources of the Heidelberg-Moscow experiment . . . . .	14
3.2	Background simulations . . . . .	17
3.2.1	The internal background from cosmogenic isotopes . . . . .	17
3.2.2	External background . . . . .	20
3.3	Background summary . . . . .	25
3.4	Performance with instrumented shield for LAr . . . . .	26
<b>4</b>	<b>Physics reach</b>	<b>29</b>
4.1	Phase I . . . . .	29
4.2	Phase II . . . . .	30
<b>5</b>	<b>Technical aspects of the experiment</b>	<b>31</b>
5.1	Overview . . . . .	31
5.2	Cryogenic tank options . . . . .	32
5.2.1	Superinsulated vessel . . . . .	33
5.2.2	Flat bottom tank . . . . .	34
5.2.3	Conclusions . . . . .	39
5.3	Detector suspension . . . . .	39
5.4	Lock and cleanroom . . . . .	40
5.5	Neutron and muon shield . . . . .	41
5.6	Electronic readout . . . . .	43
5.7	Data acquisition and Slow Control . . . . .	44
5.8	Liquid gas purification . . . . .	45
5.8.1	Noble gas adsorption . . . . .	45
5.8.2	Monitoring of liquid gas purity . . . . .	47
5.9	Water purification . . . . .	48
5.10	Liquid gas storage . . . . .	48
<b>6</b>	<b>Procurement of enriched <math>^{76}\text{Ge}</math> detectors</b>	<b>49</b>
6.1	Modification of existing $^{76}\text{Ge}$ detectors . . . . .	49
6.2	Fabrication of enriched $^{76}\text{Ge}$ detectors . . . . .	50
6.2.1	Procurement of enriched $^{76}\text{Ge}$ . . . . .	50
6.2.2	Processing of $^{76}\text{GeO}_2$ to intrinsic $^{76}\text{Ge}$ crystals . . . . .	51
6.2.3	Detector fabrication . . . . .	51

6.2.4	Loss of $^{76}\text{Ge}$ material during processing . . . . .	52
<b>7</b>	<b>R&amp;D program</b>	<b>53</b>
7.1	Mechanical engineering . . . . .	53
7.2	Electronic engineering . . . . .	53
7.3	Monte Carlo simulations . . . . .	54
7.4	Validation of materials . . . . .	54
7.5	Detector R&D . . . . .	55
7.6	Germanium enrichment . . . . .	55
7.7	Instrumentation of liquid argon . . . . .	56
<b>8</b>	<b>Safety</b>	<b>58</b>
<b>9</b>	<b>Time schedule</b>	<b>62</b>
	<b>References</b>	<b>64</b>

# 1 Overview and executive summary

**The physics case.** Since their discovery neutrinos have been an object of extensive experimental study and the knowledge about their properties has advanced our understanding of weak interactions significantly. Still unanswered, however, is the very fundamental question whether the neutrino is a Majorana particle like most extensions of the Standard Model assume. The study of neutrinoless double beta decay is the most sensitive approach to answer this question and the potential of this method has increased considerably during the last years since a non-zero mass of the neutrinos has been established by the observation of neutrino flavor oscillation. In fact, the observation of neutrinoless double beta decay would not only establish the Majorana nature of the neutrino but also provide a measurement of its effective mass.

Recently, the group of Klapdor-Kleingrothaus has claimed for the first time positive indications for neutrinoless double beta decay of  $^{76}\text{Ge}$  [Kla 04]. In this Letter of Intent we propose a new facility at the Laboratori Nazionali del Gran Sasso (LNGS) which will allow to study decays of  $^{76}\text{Ge}$  at unprecedented low background levels.

**The experimental situation.** At present the most sensitive experiments – Heidelberg-Moscow and IGEX – use  $^{76}\text{Ge}$  as source and detector, and reach sensitivities around 0.3 eV in the effective neutrino mass. Both collaborations have reported almost the same upper limit on the lifetime of  $1.6 \cdot 10^{25}$  y, corresponding to a mass range of 0.33 to 1.3 eV. However, the group of Klapdor-Kleingrothaus claims a  $4 \sigma$  excess in the spectrum near the energy expected for neutrinoless double beta decay, and gives a neutrino mass range from 0.2 eV to 0.6 eV. Currently, no other experiment can either confirm or refute this observation. Closest to this reach are cosmological limits based on the amplitude of higher frequencies in the spatial distribution of galaxies; streaming of mass-less neutrinos should reduce the spectral power at high frequency. WMAP has given upper mass limits of 0.23 eV per species [Spe 03]. Other authors have pointed out that this value is model-dependent, and that more conservative estimates give higher values [Elg 03]. However, data have also been interpreted as showing positive evidence of massive neutrinos [All 03]. Double beta decay experiments now taking data such as CUORICINO [Arn 03] or NEMO [Arno04] may reach the 0.3 eV sensitivity region within a few years, using other nuclei as sources. These experiments have the potential to confirm the current positive evidence with similar significance, but cannot refute it because of uncertainties in the ratio of nuclear matrix elements. On a similar time scale the KATRIN experiment [Osi 01] will reach a mass sensitivity of 0.2 eV to 0.3 eV based on the study of the tritium beta decay spectrum near the end point. A positive signature by KATRIN together with a sufficiently sensitive experiment on neutrinoless double beta decay would establish the Dirac or Majorana nature of neutrinos. Regardless of the outcome of these experiments, it is clear that a  $^{76}\text{Ge}$  experiment capable of confirming the current result with high significance, or pushing the mass limits below the current, cosmologically still important 0.3 eV range is of high scientific relevance.

**The new low-level facility based on a cryogenic fluid shield.** In an experiment searching for neutrinoless double beta decay, the number of decays expected is proportional to the detector mass  $M$  and the measurement time  $T$ . The crucial factor determining the performance of the experiment is the background in the mass window of the neutrinoless double beta decay line. As long as there are no background counts, lifetime limits improve as  $(MT)$  whereas in the presence of background limits go as  $(MT)^{1/2}$ . Thus, background suppression is the key to a successful experiment. Background spectra in current  $^{76}\text{Ge}$  experiments point to the shielding material as the dominant source of residual background. Therefore, it was proposed already several years ago to operate bare germanium diodes in a shield of liquid nitrogen [Heu 95]; the GENIUS and GEM proposals [Kla 99, Zde 01] were based on this idea. Since nitrogen can be purified extremely well from radioactive contaminants, it is one of the radio-purest environments possible and should allow a background reduction by two to three orders of magnitude compared to past  $^{76}\text{Ge}$  experiments. This allows background-free measurements up to lifetimes well beyond  $10^{26}$  years. Reliable operation of germanium detectors in liquid nitrogen and liquid argon has been demonstrated in several laboratory experiments and, on a larger scale, in the GENIUS Test Facility [Kla 03a]. Additional suppression of external and internal backgrounds can be achieved by vetoing techniques, using veto signals from other nearby detectors, from other segments of the same detector in case of segmented detectors, from the pulse shape which indicates multiple interaction sites within a detector or detector segment, or from scintillation light in the surrounding liquid in case liquid argon is employed instead of liquid nitrogen.

We propose to install a novel facility based on an (optionally active) cryogenic fluid shield in Hall A of the Gran Sasso Laboratory. The facility serves a dual purpose. The setup allows to scrutinize with high significance on a short time scale the current evidence for neutrinoless double beta decay of  $^{76}\text{Ge}$  using the existing  $^{76}\text{Ge}$  detectors from the previous Heidelberg-Moscow and IGEX experiments. An increase in the lifetime limit can be achieved by adding more enriched detectors, remaining thereby background-free up to a few 100 kg-years of exposure. On the other hand, it is a pioneering low-level facility in that it allows to develop and test low-background measurements with Germanium detectors at background levels several orders of magnitude below the current state-of-the-art; it represents a major step on the way towards ultimate double beta decay experiments aiming for a sensitivity in the 10 meV mass range.

For cost and space reasons, we consider to use a combination of shields, rather than a single thick liquid nitrogen shield as in the original GENIUS proposal [Kla 99]. While the optimum shield configuration is still under investigation, a promising layout is to use a 1.5 m liquid nitrogen shield followed by a  $\approx 10$  cm shield of high-purity lead still inside the cryostat. The lead shields activity from the cryostat walls and insulation material and results in a compact cryostat, important both for cost and safety aspects, since the volume of the cryogenic fluid is kept relatively small. The thickness of the liquid is chosen to sufficiently shield remaining activities in the lead. An outer shield of roughly 2 m of water complements the shielding against the rock and concrete. It also serves as a neutron shield and – encased in a diffuse reflecting foil and equipped with photomultipliers – as a veto against cosmic muons. A cleanroom and sophisticated lock and suspension systems

on top of the cryostat allow to insert and remove detectors without introducing contamination into the vessel. Gas purification and handling systems make extensive use of the experience accumulated in BOREXINO. Signal recording and pulse shape analysis make use of recent developments where signals are sampled and digitized at high rate after minimal analog signal processing, providing maximal information and flexibility for a later digital post-processing.

**Phases of the experiment.** The experiment would proceed in several phases.

Phase I encompasses the installation of the cryostat and shields, the installation and operation of conventional Ge detectors to determine the background rejection and to screen materials and identify backgrounds by classifying their spectra, and the operation of almost 20 kg of existing enriched  $^{76}\text{Ge}$  detectors, used in the past in the Heidelberg-Moscow and IGEX experiments. Within one year of measurement, the sensitivity of this setup should allow a statistically unambiguous statement concerning neutrinoless double beta decay with a lifetime around  $1.2 \cdot 10^{25}$  y, as measured by [Kla 04].

Phase II: In parallel with the data taking of the first phase, techniques will be studied and implemented to provide improved enriched detectors to be used in a second phase. Enriched germanium will be produced in Russia; two different options to enrich the germanium are under discussion. Detector geometry and segmentation will be optimized on the basis of detailed calculations of fields and pulse shapes, taking into account background simulations. Particular emphasis is devoted to minimize cosmogenic activation of detectors by reducing the exposure and optionally moving production steps to underground facilities. Regardless of the outcome of the Phase I measurements, it is desirable to produce and operate a certain number of new detectors: In case of a positive result to provide a precise lifetime measurement, in case of a negative outcome to push the limits further. In particular in the second case, one would – funding permitting – add enriched detectors up to the point where backgrounds start to show up.

At the end of Phase II with 100 kg·years, the sensitivity will be  $T_{1/2} > 2 \cdot 10^{26}$  years at 90% confidence level (C.L.) corresponding to a range of the effective neutrino mass of  $< 0.09 - 0.29$  eV.

Phase III: The ultimate experiment capable to reach the 10 meV scale requires  $\mathcal{O}(1 \text{ t})$  of enriched germanium and represents another huge step, which can only be afforded in the context of a world-wide collaboration. Options for detector shielding and detector arrangements will have to be reevaluated on the basis of results achieved by the proposed experiment and by studies following other approaches, such as the copper shield foreseen in the Majorana proposal [Maj 03]. It is likely that by that time the proposed facility will have reached its limits - in fiducial size, in background shielding, or in both – and needs to be upgraded or replaced by an improved facility. On the scale of the cost of 1 t of enriched germanium, costs for such a new facility are modest. At the current time, it is, however, clearly premature to speculate about the kind of modifications needed, or the space required by and the potential location of such a future experiment.

**Time scale, cost, and requests to LNGS.** Making use of the available know-how concerning gas purification in BOREXINO, and ideally also of the BOREXINO infrastructure, we estimate that the cryostat and auxiliary system could be set up on a time scale of less than 2 years. After installation of the  $^{76}\text{Ge}$  detectors a measurement time of at least three years is required. The cost of the cryostat, the auxiliary systems and the modification of the existing detectors is estimated to be 3 M€.

Phase II – the production of new enriched detectors – could start concurrently with Phase I. Less than 3 years will be required until the first detectors are available. The cost of Phase II depends on the amount of additional detectors, and on the production mode. Detector costs are roughly 100 €/g, including the raw material, the enrichment and the crystal growing, plus a certain offset since the crystal growing requires a certain amount of additional material (which can be recovered for a second lot of detectors). Underground detector preparation would require laboratory equipment worth about 1 M€.

The facility for Phase I and II could be located in the free space in Hall A of LNGS. Electronics, experiment control and gas control could be housed partly on top of the cryostat, partly in (stacked) containers. Additional space is required for liquid gas tanks. Safety issues regarding the cryogenic fluid system and gas handling need to be addressed in close collaboration with LNGS safety officers.



## 2 Introduction and experimental overview

### 2.1 Introduction

Double beta decays are transitions between nuclei of the same atomic mass number ( $A$ ) that change the nuclear charge ( $Z$ ) by two units under emission of light particles. Double beta decay is only observable in absence of the concurring process, the cascading decay via two single beta decays. This condition is only satisfied, if the mass of the intermediate nucleus is larger than that of the initial one, or if the single beta transition to the intermediate nucleus is highly hindered. Double beta transitions for both signs of nuclear charge change are possible: two neutrons transform into two protons, or vice versa, two protons into two neutrons. For simplicity, we consider here only the first.

The transformation can occur under emission of two neutrinos ( $\beta\beta(2\nu)$ ),

$$(A, Z) \rightarrow (A, Z + 2) + e_1^- + e_2^- + \bar{\nu}_{e1} + \bar{\nu}_{e2}, \quad (1)$$

conserving lepton number. In contrast, the neutrinoless decay ( $\beta\beta(0\nu)$ )

$$(A, Z) \rightarrow (A, Z + 2) + e_1^- + e_2^- \quad (2)$$

violates lepton number by two units and is forbidden in the standard electroweak theory. A further decay mode involves the emission of a light neutral boson ( $\beta\beta(0\nu, \chi)$ ), a majoron, as postulated in some extensions of the standard electroweak theory:

$$(A, Z) \rightarrow (A, Z + 2) + e_1^- + e_2^- + \chi \quad (3)$$

The different decay modes are distinguishable by the shape of the spectrum of the electron sum energy. For the  $\beta\beta(2\nu)$  mode, the summed kinetic energy of the two electrons displays a continuous spectrum with a broad maximum below half the endpoint energy. In contrast, the  $\beta\beta(0\nu)$  mode exhibits a mono-energetic line at the endpoint ( $Q_{\beta\beta}$ ), as the electrons carry the full available energy. For a light majoron, the spectrum is also continuous with a broad peak located above half the endpoint energy.

Neutrinoless double beta decay can be mediated by various mechanism. Here we consider only the simplest case of the left-handed  $V - A$  weak currents and the exchange of a light massive Majorana neutrino. The half life is then (e.g. [Ell 02])

$$[T_{1/2}^{0\nu}(0^+ \rightarrow 0^+)]^{-1} = G^{0\nu}(E_0, Z) |M_{GT}^{0\nu} - g_V^2/g_A^2 M_F^{0\nu}|^2 m_\nu^2, \quad (4)$$

where  $G^{0\nu}$  is the phase-space integral,  $M_{GT}^{0\nu}$ ,  $M_F^{0\nu}$  are the nuclear matrix elements, and  $m_\nu$  the effective electron neutrino mass. Under the assumption of three light massive Majorana neutrinos  $\nu_i$  ( $i = 1, 2, 3$ ), the weak eigenstate neutrinos  $\nu_e, \nu_\mu$  and  $\nu_\tau$  can be written as a superposition of the mass eigenstates  $\nu_i$  with the mixing matrix  $U_{li}$ . The electron neutrino  $\nu_e$  is then given as  $\nu_e = \sum_i^3 U_{ei}\nu_i$  and the effective neutrino mass defined as

$$m_\nu^2 = \left| \sum_i^3 U_{ei}^2 m_i \right|^2 = \left| \sum_i^3 |U_{ei}|^2 e^{\alpha_i} m_i \right|^2, \quad (5)$$

including two CP violating Majorana phases  $\alpha_i$  which can cause cancellations in the sum.

From the measurements of the mass differences  $\Delta m_{ij}^2 = |m_i^2 - m_j^2|$  and the mixing angles in neutrino oscillation experiments, the range for  $m_\nu$  is substantially constrained. Figure 1 displays the range of  $m_\nu$  as a function of the lightest neutrino mass  $m_1$ . One distinguishes

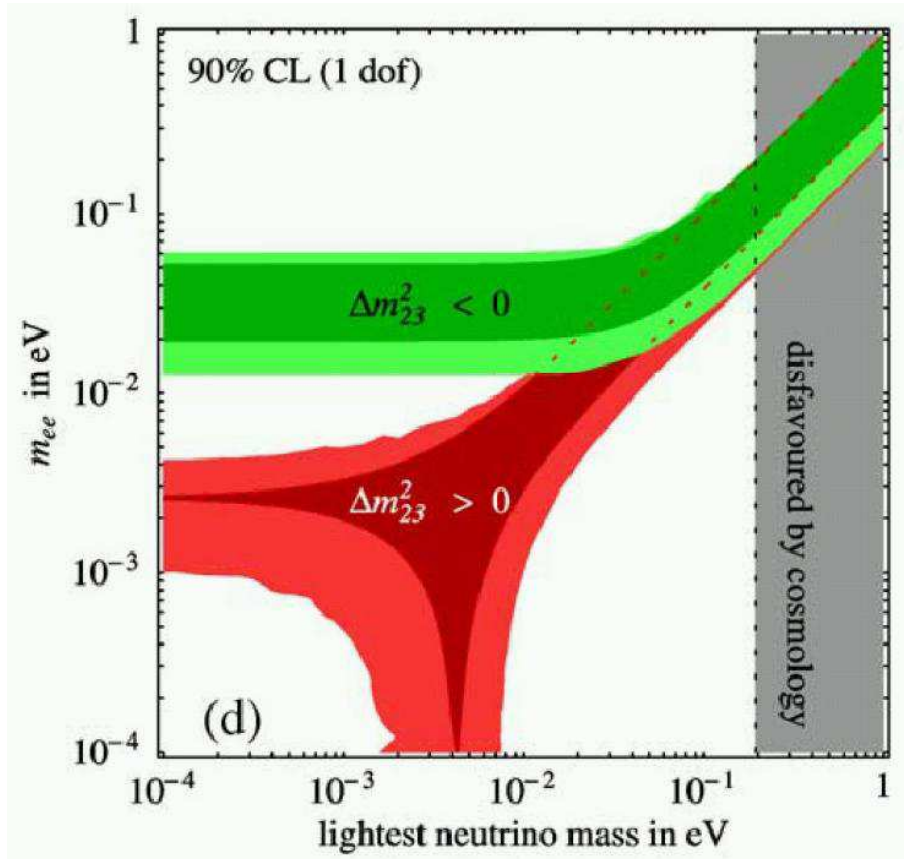


Figure 1: Predictions for the effective neutrino mass  $m_\nu$  as a function of the lightest neutrino mass  $m_1$  derived from oscillation experiments [Fer 03]. The different bands in parameter space correspond to the normal mass hierarchy ( $\Delta m_{23} > 0$ ), to the inverted mass hierarchy ( $\Delta m_{23} < 0$ ) and to the degenerate mass scheme (lightest mass  $\gg \Delta m_{23}$ ). The dark colors use the measured oscillation data without errors to emphasize the contribution of the Majorana CP phases. The lighter colors include the current experimental errors of the mixing parameters.

the parameter range corresponding to normal, inverted and degenerated mass schemes. In the normal hierarchy, the mass splitting driving solar neutrino oscillations occurs between the lightest neutrino  $m_1$  and  $m_2$ , and that driving atmospheric oscillations between  $m_2$  and  $m_3$ . In the inverted hierarchy the splitting is arranged in the reverse order. If the values of  $\Delta m_{ij}^2$  are small compared to the actual values of  $m_i$ , the mass spectrum is called degenerate. Large parts of the parameter space for  $m_\nu^2$  predicted by neutrino oscillation

experiments will be experimentally accessible with the next generation of experiments.

## 2.2 Past and present experiments

Major experimental progress has been achieved during the last ten years. For a comprehensive review the reader is referred to [Ell 02]. Direct measurements of double beta decay accompanied by the emission of two neutrinos ( $\beta\beta(2\nu)$ ) have been carried out for more than ten nuclei. Recent results for  $\beta\beta(2\nu)$  include  $^{76}\text{Ge}$ ,  $^{100}\text{Mo}$ ,  $^{150}\text{Nd}$ ,  $^{116}\text{Cd}$  and  $^{96}\text{Zr}$ . The measured half-lives are in the range of  $10^{19} - 10^{21}$  years.

Today the central focus in double beta decay research is the neutrinoless mode ( $\beta\beta(0\nu)$ ). Most stringent limits have been derived from experiments using enriched  $^{76}\text{Ge}$  detectors. The leading two experiments - IGEX and Heidelberg-Moscow (HdM) - have been running for several years with a background around  $Q_{\beta\beta}$  close to 0.2 cts/(keV·kg·y) before pulse shape discrimination and about 0.06 cts/(keV·kg·y) after. Limits for the life time close to  $2 \cdot 10^{25}$  y have been derived corresponding to a limit for an effective neutrino mass  $m_\nu$  of 0.3 - 1.0 eV [Aal 99, Kla 01]. Both experiments have stopped data taking recently.

In 2001, the group of Klapdor-Kleingrothaus claimed evidence for neutrinoless double beta decay at a  $2 \sigma$  confidence level [Kla 01] based on 52 (kg·y) of data from the HdM experiment. Based on a data set of 72 (kg·y) the claim has been strengthened recently [Kla 04]. The derived excess counts are  $28.8 \pm 6.9$  events above a background of approximately 60 events.

Operational experiments are currently NEMO3 and CUORICINO. The NEMO experiment is carried out at the Frejus Underground Laboratory, France. During five years of R&D phase using the NEMO2 detector, the collaboration has performed measurements of the  $\beta\beta(2\nu)$  decay of  $^{100}\text{Mo}$ ,  $^{82}\text{Se}$ ,  $^{116}\text{Cd}$  and  $^{96}\text{Zr}$ . The final detector, NEMO3 [Arno04], consists of a large tracking calorimeter surrounding 10 kg of thin source foils of different enriched materials, mainly 7 kg of  $^{100}\text{Mo}$ . The aim is to reach after five years of data taking a limit for the half-life of  $5 \cdot 10^{24}$  years, corresponding to an effective mass of 0.2-0.3 eV. NEMO3 started data taking in 2003.

The CUORICINO experiment at LNGS searches for neutrinoless double beta decay with  $\text{TeO}_2$  bolometers [Arn 03]. The setup consists of an array of 62 crystals with a total mass of about 40 kg. The counting rate in the region of neutrinoless double beta decay is  $\sim 0.2$  cts/(keV·kg·y). No evidence for neutrinoless double beta decay is found with the present exposure of about three months during 2003. The corresponding limit for the lifetime is  $5.5 \cdot 10^{23}$  y (90% C.L.) and for the effective neutrino mass between 0.37 and 1.9 eV [Arn 04]. The expected sensitivity after three years of data taking will be  $4 \cdot 10^{24}$  y or 0.2-0.5 eV [Giu 03].

## 2.3 Proposed and suggested future experiments

The next generation of double beta decay experiments aims for probing Majorana masses down to 0.1 eV and below. Many different isotopes and detector concepts have been suggested. Recent reviews of the field can be found in [Ell 02, Giu 03]. Here, we briefly

discuss the more advanced projects as listed in Tab. 1 including this proposed new  $^{76}\text{Ge}$  experiment at LNGS.

Table 1: Characteristics of operating and proposed future  $\beta\beta(0\nu)$  experiments. The corresponding references are: NEMO3 [Aug 03], CUORICINO [Giu 03], NEMO-Next [Aug 03], CUORE [Arn 03], MAJORANA [Maj 03], EXO [Dan 00]. The three phases of the proposed  $^{76}\text{Ge}$  experiment are discussed in the following sections.

Experiment	Source	Description	FWHM at $Q_{\beta\beta}$ (keV)	Sensitivity		Year
				$T_{1/2}^{0\nu}$ (y)	$m_\nu$ (eV)	
NEMO3	$^{100}\text{Mo}$	7 kg $^{enr}\text{Mo}$ tracking	90	$5 \cdot 10^{24}$	0.2-0.3	2008
CUORICINO	$^{130}\text{Te}$	40 kg $\text{TeO}_2$ bolom.	7	$4 \cdot 10^{24}$	0.2-0.5	2007
NEMO-Next	$^{100}\text{Mo}$	0.1 t $^{enr}\text{Mo}$ track.	50	$1 \cdot 10^{26}$	0.04-0.07	
CUORE	$^{130}\text{Te}$	0.76 t $\text{TeO}_2$ bolom.	5	$3 \cdot 10^{26}$	0.03-0.05	
MAJORANA	$^{76}\text{Ge}$	0.5 t $^{enr}\text{Ge}$ diodes	4	$4 \cdot 10^{27}$	0.02-0.07	
EXO	$^{136}\text{Xe}$	1 t $^{enr}\text{Xe}$	120	$8 \cdot 10^{26}$	0.05-0.14	
This Project	$^{76}\text{Ge}$	$^{enr}\text{Ge}$ in LN/LAr	4			
Phase I		15 kg (15 kg y)		$3 \cdot 10^{25}$	0.3-0.9	2006
Phase II		35 kg (100 kg y)		$2 \cdot 10^{26}$	0.09-0.29	2009
Phase III		$\mathcal{O}(500 \text{ kg})$ - world-wide collaboration				

NEMO-Next would be based on the NEMO3 tracking concept, however with an increased mass of approximately 100 kg of foils enriched in  $^{100}\text{Mo}$  and improved energy resolution. A sensitivity of  $> 10^{26}$  y or of 0.04 – 0.07 eV for  $m_\nu$  is projected.

The Cryogenic Underground Observatory for Rare Events (CUORE) has been proposed to be operated at the Gran Sasso laboratory. It is planned to use 1000 crystals of  $\text{TeO}_2$  with a total mass of 760 kg as cryogenic bolometers [Arn 03]. The detector is arranged into 25 separate towers of 40 crystals. A prototype tower is operated in CUORICINO. Assuming an energy resolution of 5 keV and a background of 0.01(0.001) cts/(keV·kg·y), the expected sensitivity of CUORE is  $0.9(3.0) \cdot 10^{26} \sqrt{t}$  years. One year of measurements would provide bounds for  $m_\nu$  in the 0.04 – 0.15 eV range [Arn 03].

The MAJORANA experiment plans to employ 500 kg of Ge, isotopically enriched to 86% in  $^{76}\text{Ge}$ , in the form of about 200 detectors in a densely packed array. Each crystal will be segmented, and the signals from each segment will be subjected to pulse shape analysis. A half-life sensitivity is predicted of  $4 \cdot 10^{27}$  y or 0.02 - 0.07 eV for  $m_\nu$  after approximately ten years of operation.

The Enriched Xenon Observatory (EXO) proposes to use 1-10 tons of xenon enriched to 60-80 % in  $^{136}\text{Xe}$ . In contrast to other proposals, it is planned to discriminate backgrounds by identification of the daughter isotope  $^{136}\text{Ba}$  with laser spectroscopic methods. If realized successfully, all backgrounds but the  $\beta\beta(2\nu)$  mode could be suppressed. Two different detector concepts are under study: high-pressure gas TPC or liquid xenon scintillator.

Sensitivities of  $8 \cdot 10^{26}$  y, or  $0.05 - 0.14$  eV for  $m_\nu$ , are projected.

Other interesting projects have been proposed including MOON [Eji 00] (34 t of natural molybdenum in a sandwich Mo/scintillator configuration), CAMEO [Bel 01] (1 t of scintillating  $^{116}\text{CdWO}_4$  crystals situated within the BOREXINO detector), and COBRA [Zub 01] (CdTe or CdZnTe semiconductors).

In the new  $^{76}\text{Ge}$  initiative at the LNGS, presented in this Letter of Intent, we intend to operate bare germanium diodes enriched to 86% in  $^{76}\text{Ge}$  in a high-purity cryogenic medium for shielding against external radiation. The concept, detailed in the following sections, is based on the observation that the background signals are largely dominated by external radiation. By removing most of the cladding and contact materials, and immersing the crystals in an ultra-pure environment, one can operate the diodes largely free of background. Provided that the background can be reduced to  $10^{-3}$  cts/(keV·kg·y), it will be possible to operate crystals free of backgrounds up to exposures of 100 (kg·y). The experimental strategy is based on three phases, in each incrementing the target mass. In Phase I it is planned to operate the existing almost 20 kg enriched germanium detectors which have been used in the IGEX and Heidelberg-Moscow experiment. Conservatively, it is assumed that 15 out of almost 20 kg will be operational. About 20 kg of additional  $^{76}\text{Ge}$  crystals are conceived for Phase II. The third phase has to be defined during Phase II and depends on the physics result and the experimental performance. Already after completion of Phase I, it will be possible to test the recent claim of evidence for neutrinoless double beta decay.

### 3 Design considerations: background sources and discrimination methods

The main prerequisite for a next generation experiment is a background reduction by two to three orders of magnitude compared to existing experiments. A background index of less than  $10^{-3}$  cts/(keV·kg·y) is the goal. This and the cost of the experiment are the prime design considerations. In addition, the available space in Gran Sasso Hall A constrains the design.

While such a tremendous background reduction is difficult to predict reliably, the contributions of many well identified background sources can be extrapolated with Monte Carlo techniques. Shielding of the germanium diodes with ultra-pure material, such as liquid nitrogen (LN) or liquid argon (LAr), is one of the key prerequisites [Heu 95]. Following this idea the GENIUS [Kla 99] and GEM [Zde 01] experiments were proposed. A more conventional approach with shielding by copper and lead is pursued by the MAJORANA collaboration [Maj 03].

For the proposed experiment, a combination of the different shielding methods is foreseen. The germanium is immersed in liquid nitrogen or argon, but some of the shielding is achieved by lead and water. Fig. 2 shows schematically such a design. In this section different background sources and vetoing techniques are discussed. The various options for the realization of the experimental setup will be presented in section 5.

This section starts with a discussion of the understanding of the background seen in the Heidelberg-Moscow experiment in the relevant energy region from 2.0 to 2.1 MeV. Afterwards, the background from external sources and from sources intrinsic to the detectors are discussed. Finally, this section ends with a discussion of the potential of scintillation light detection in LAr.

#### 3.1 Background sources of the Heidelberg-Moscow experiment

A good understanding of the available data is needed to estimate the background rejection of the future experiments, especially as the existing enriched germanium diodes are used in the first phase of the experiment. The experimental setup of the Heidelberg-Moscow experiment consisted of 5 copper cryostats, each of them housed an enriched  $^{76}\text{Ge}$  diode. Four of the detectors were operated in a common lead shield while one detector (no. 4) was operated in a separate shield of copper and lead [Kla 03].

Fig. 3 shows the simulated background spectrum in the energy range from 2000 to 2100 keV of the Heidelberg-Moscow experiment [Kla 03, Dör 03]. It identifies the primordial decay chains of U and Th as the main contamination sources, with 38% and 41%, respectively. Smaller background contributions originate from the cosmogenic radio-nuclide  $^{60}\text{Co}$  (16%), anthropogenic contaminations and neutron/muon (in situ) induced events (5%).

The background contributions are estimated by fitting the peak count rates and Compton distributions of simulated spectra for the individual backgrounds to the total measured

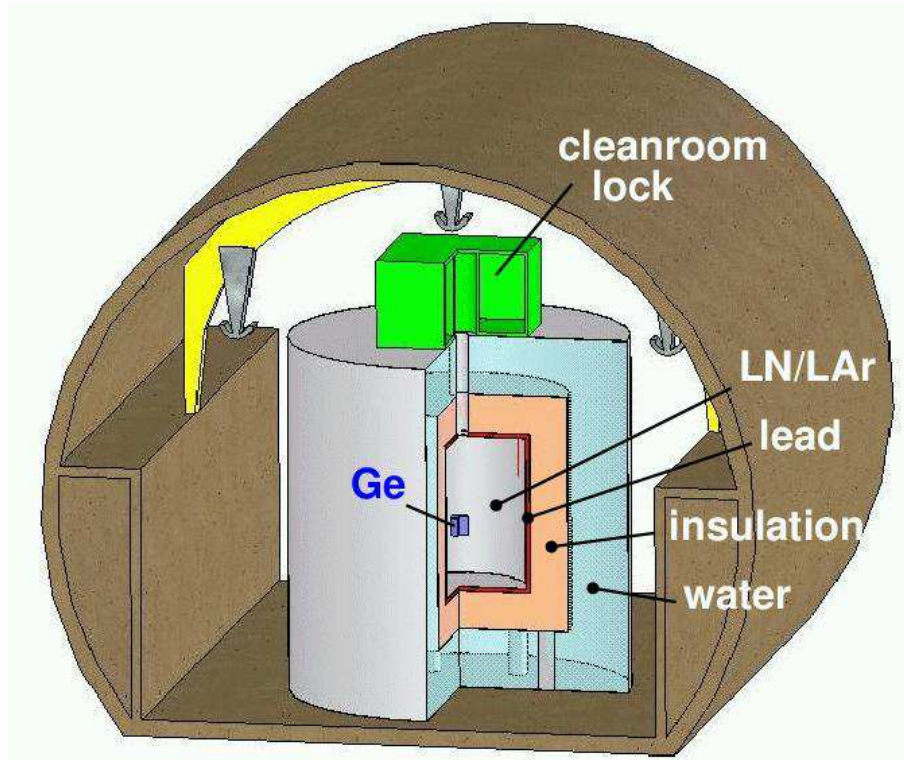


Figure 2: Schematic drawing of the tank in Gran Sasso Hall A. In the middle of the tank the Ge diode setup is immersed in the liquid nitrogen or liquid argon (LN/LAr). Following from the inside to the outside is a layer of lead, thermal insulation and a water shield. The outer diameter is 10 m.

spectrum (from about 50 to 2700 keV, 49.59 kg y). In case of a source emitting gamma cascades, like the U/Th chain, the measured energy spectrum depends sensitively on the distance between source and detector showing e.g. summation peaks of different intensities. This effect has been used to localize the contaminations within the detector cryostats and the shielding material. It is found that the predominant fraction of the U/Th contamination is located at the copper parts of the cryostats. The same holds also for K contributions, but due to its single  $\gamma$  line the assignment was more indirect. The sum of the simulated backgrounds is  $660 \pm 93$  events while the data spectrum has 803 entries [Dör 03]. Thus the simulation has large uncertainties and does not explain the data entirely.

The cosmogenic activities originate from  $^{60}\text{Co}$  decays and are dominantly located in the copper of the cryostats [Die 99]. The upper limits for the fraction of decays inside the diodes are between 1.1% and 7.4%. Consequently, there is no evidence for background sources inside the crystals in the energy interval of interest.

Table 2 compares the activities obtained for the copper of the individual cryostats [Dör 03] with the directly measured activities of the same copper quality by the Ge spectrometer GeMPI [Ned 00]. GeMPI is also operated at the LNGS at an even lower back-

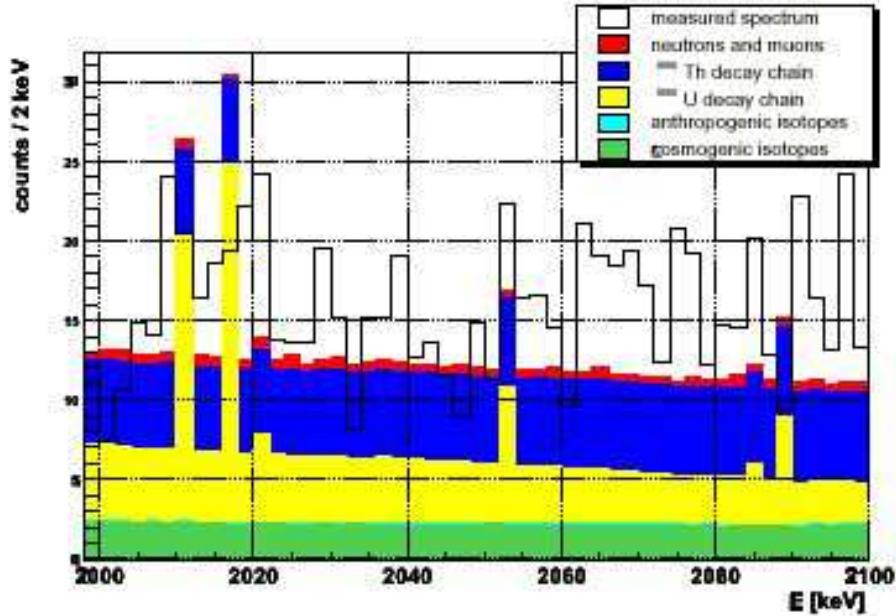


Figure 3: Simulated background of the Heidelberg-Moscow experiment in comparison with the measured spectrum [Kla 03, Dör 03]. The background labeled “cosmogenic isotopes” refers to  $^{60}\text{Co}$  decays in the copper cryostats.

ground level than the Heidelberg-Moscow detectors. Its sample chamber allows to place large sample quantities around the detector, for example, 125 kg of Cu in this case. The strong variation of the activities from cryostat to cryostat, which are in most cases higher than the upper limits of the bulk measurement with GeMPI, suggest that the contaminations are not intrinsic to the copper but are rather located on the surface. A clear indication of variable surface contamination is given by the different  $^{210}\text{Po}$   $\alpha$  peak heights measured in the high energy spectra of the five enriched detectors. This contamination which is caused by impurities on the surface of the p-contacts of the crystals varies by a factor of 30 [Die 99].

In the liquid nitrogen immersion method the direct cladding material will be reduced by about 4 orders of magnitude in weight and by about a factor of 200 in surface (not counting the crystal surface itself). The dominant remaining background will be intrinsic to the diodes. Since there is no evidence for this contamination, a factor of 20 in background reduction is assumed in the calculation of the physics reach for the first phase of the experiment.

An independent background analysis of the Heidelberg-Moscow data by members of the Moscow group is ongoing. The method is very similar to the one outlined above but separates bulk and surface contaminations in the simulations. Final results are expected soon.



Table 2: Contaminations of the copper [ $\mu\text{Bq}/\text{kg}$ ] in the various cryostats of the Heidelberg-Moscow experiment. The values are deduced from a Monte Carlo simulation of measured spectra [Dör 03]. For comparison the corresponding values measured with the GeMPI facility are shown.

	$^{226}\text{Ra}(\text{U})$	$^{228}\text{Th}(\text{Th})$	$^{40}\text{K}$
Cryostat of ANG1	$168\pm 8$	$84\pm 7$	$236\pm 61$
Cryostat of ANG2	$91\pm 4$	$10\pm 3$	$78\pm 22$
Cryostat of ANG3	$105\pm 5$	$84\pm 5$	$927\pm 46$
Cryostat of ANG4	$115\pm 3$	$87\pm 4$	$199\pm 04$
Cryostat of ANG5	$100\pm 4$	$26\pm 4$	$1632\pm 49$
same Cu quality measured with GeMPI	$\leq 20$	$\leq 23$	$\leq 88$

## 3.2 Background simulations

Several sources of background have been identified by past experiments. These can be classified by the location of the radioactive isotope: internal to the germanium diode or external in the material for shielding, in the contacts and in the concrete/rock of the laboratory.

This section focuses on the simulation of the backgrounds considered to be most serious. A more complete list will be given in a later document. The discussion of the internal background applies to newly built detectors (Phase II of the experiment) while the external backgrounds affect the design of the tank.

For a detailed simulation GEANT4 version 5.2 patch 2 was used. Only a simplified setup consisting of a tank for liquid nitrogen or argon, the liquid and an ensemble of 27 germanium detectors was simulated. Each detector has a height of 78 mm and a diameter of 78 mm which corresponds to a weight of 2 kg. The detectors will be “p-type” and hence a dead layer of 0.7 mm at the outside was included in the simulation. In the middle, a cylindrical hole of 10 mm diameter and a length of 58 mm is included for the p contact. The crystals are arranged in a  $3 \times 3 \times 3$  array with a spacing of 12 mm.

In addition a CPU time optimized Monte Carlo for extensive simulations of gamma interactions is used. This program simulates Compton scattering, pair production and photo electric effect and performs about a factor of 30 faster than GEANT4. However, only geometries with a single diode have been implemented. Simulations were carried out for internal as well as for external background.

### 3.2.1 The internal background from cosmogenic isotopes

During storage at sea level the germanium is exposed to hadronic radiation, especially neutrons. These cause spallation in the germanium and hence a variety of radioactive

isotopes are produced. These processes can be simulated and past experience shows that the results of simulations agree with measurements within a factor of two [Avi 92, Mai 96].

Most relevant for the neutrinoless double beta decay are the decays of  $^{68}\text{Ge}$  and  $^{60}\text{Co}$  since  $Q$  values above  $Q_{\beta\beta} = 2039$  MeV occur in the decay chain, and the lifetimes are in the range of years.

### *Cosmogenic $^{60}\text{Co}$ background in the germanium diode*

The cosmogenic production of  $^{60}\text{Co}$  in a germanium detector is about 4 atoms/(kg d) at sea level [Avi 92]. Therefore an exposure of one day corresponds to an activity of  $4 \ln(2)/T_{1/2} = 0.017 \mu\text{Bq/kg}$ . This number agrees within a factor of 1.6 with the value from reference [Bau 99].<sup>1</sup>

If the detectors are fabricated underground, an exposure time of 10 days after zone refinement may be realistic and shall be used here. Since the zone refinement will largely remove the  $^{60}\text{Co}$  atoms, the exposure time results in an activity of  $0.17 \mu\text{Bq/kg}$  which corresponds to 5.4 decays/(kg y). Fig. 4 shows the simulated energy deposited inside the diode. In one out of 6000 decays the deposited energy is at  $Q_{\beta\beta}$  within a 1 keV window. The resulting background index is therefore  $0.9 \cdot 10^{-3}$  cts/(keV·kg·y). Most of these events can be rejected by requiring an anti-coincidence with other detectors and for segmented detectors by an anti-coincidence of the segments. If the decay occurs in the inner crystal of the simulated setup and if the deposited energy is close to  $Q_{\beta\beta}$ , in about 85% of the events some energy is deposited in a second crystal. For a detector at the corner about half of the events have energy deposition in a second crystal.

Another proposed background rejection method is the segmentation of the detector contact which allows for a better localization of the energy deposition. Since electrons will deposit their energy very localized, the anti-coincidence of segments can be applied. For a four-fold segmentation along the axis of the diode (axial segmentation) an additional suppression of about 5 can be expected. Slightly worse numbers apply for a four-fold azimuthal segmentation (pie slices). In total a factor of 30 in background suppression can be achieved (for the center crystal) by the anti-coincidence method.

Pulse shape analysis provides an additional mean to suppress background. This has not been studied so far but is expected to result in an additional rejection factor of more than 2. Beside the methods used in previous Ge experiments or proposed for the MAJORANA experiment [Maj 03, Kla 04], there is also the possibility to extend the method used by the GNO experiment for the discrimination of multiple site events in proportional counters [Pan 04].

If LAr is used as the cryogenic fluid, the detection of scintillation light would be a powerful discrimination method. According to simulations (see section 3.4) the  $^{60}\text{Co}$  background at  $Q_{\beta\beta}$  can be suppressed by a factor of 100. The ultimate limit is given by the thickness of the dead layer at the outer surface of the detector.

---

<sup>1</sup>The value given in reference [Bau 99] of  $0.18 \mu\text{Bq/kg}$  after a 10 day exposure and 3 years of storage underground corresponds to  $0.027 \mu\text{Bq/kg}$  for a one day exposure without underground decay time.

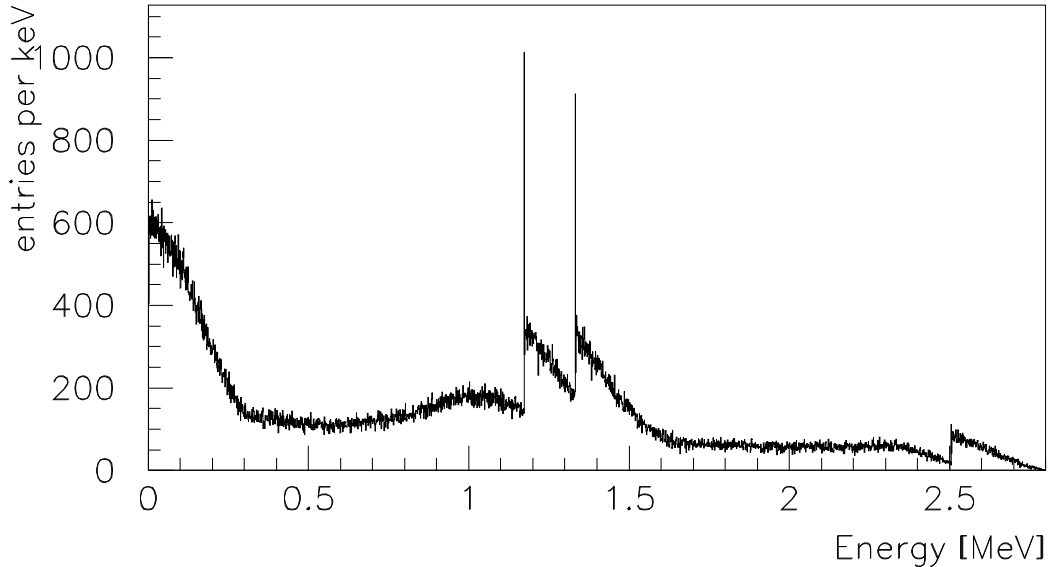


Figure 4: Energy deposition in a germanium detector from  $^{60}\text{Co}$  decays located inside the crystal. The decay chain starts with a  $\beta^-$  emission of an endpoint energy of 300 keV followed by two prompt  $\gamma$  quanta of 1.173 and 1.332 MeV.

#### *Cosmogenic $^{68}\text{Ge}$ background in the germanium diode*

According to calculations in reference [Avi 92], the production rate of  $^{68}\text{Ge}$  in  $^{76}\text{Ge}$  is about 1 atom/(kg d). Here the time since the last isotope separation step is relevant. Even if the detector is fabricated underground the activation time could be several months. Since  $T_{1/2} \sim 270$  d, the activation will be a large fraction of the saturation activity. Here we will assume 180 days for the time between the isotope separation and the storage underground. This results in 40% of the saturation activity.

The saturation activity corresponds to 1 decay/(kg d) at the time the detector is brought underground. This corresponds to 400  $^{68}\text{Ge}$  atoms/kg, and 60% of these will decay in the first year. Fig. 5 shows the spectrum of deposited energy. In about one out of 5000 decays the energy is within 1 keV of  $Q_{\beta\beta}$ . This yields a background of  $19 \cdot 10^{-3}$  cts/(keV·kg·y) which is obviously not acceptable. Several methods exist to reduce this background:

- Waiting: the small half life makes waiting an option. After three years the activity is 1/16.
- Anti-coincidence of detectors: the  $\beta^+$  decay of  $^{68}\text{Ga}$  yields two 511 keV photons from positron annihilation. These will often deposit energy in neighboring detector. For the central detector the anti-coincidence would result in a reduction by a factor 2.5. For a decay in an outer detector the background is reduced by a factor of 1.4.

- Anti-coincidence of segments: the four-fold axial segmentation yields an additional suppression factor of 4.5.
- Anti-coincidence with scintillation light in case the cryogenic fluid is LAr.
- Tagging the  $^{68}\text{Ge}$  decay to  $^{68}\text{Ga}$  and vetoing the subsequent  $^{68}\text{Ga}$  decay: About 86% of the  $^{68}\text{Ge}$  decays occur via electron capture from the K shell which results in a  $\sim 10$  keV energy deposition when the empty K shell location is filled. The  $\beta^+$  decay of  $^{68}\text{Ga}$  follows with a half lifetime of  $T_{1/2} = 68$  min. The time correlation of the two decays is therefore a powerful rejection tool. Consequently, a factor of 5 in background rejection is feasible.

Using these rejection factors, the background index in the first year (for the central crystal) can be reduced to  $0.3 \cdot 10^{-3}$  cts/(keV·kg·y) and falls exponentially with  $T_{1/2} \sim 270$  days.

As before, the background discrimination potential from the pulse shape analysis has not been explored yet.

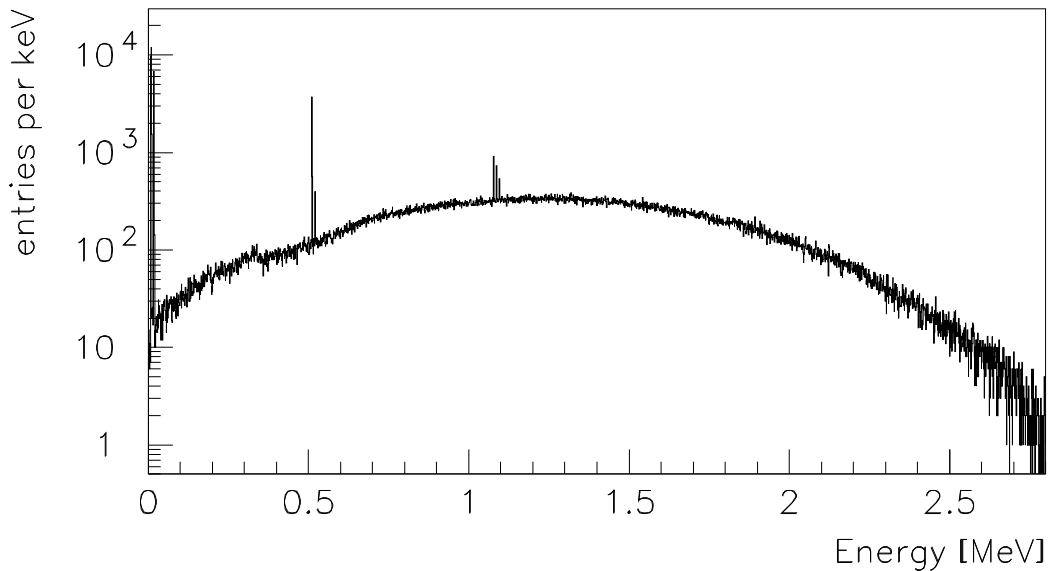


Figure 5: Energy deposition in a germanium detector from  $^{68}\text{Ga}$  decays inside the crystal.

### 3.2.2 External background

The external background consists of photons from primordial decay chains, neutrons and muon induced background. So far, most of our emphasis is focused on the suppression of

the 2.615 MeV photon from the  $^{208}\text{Tl}$  decay. This background influences the design of the tank considerably.

### *$^{208}\text{Tl}$ background*

The activity in the concrete and the rock in LNGS from  $^{208}\text{Tl}$  results in a flux of about  $1.4 \cdot 10^7$  decays/(d m<sup>2</sup>) [Arp 92]. For a cylindrical tank with 8 m inner diameter and 8 m height this corresponds to a total flux of  $1.5 \cdot 10^{12}$  photons per year.

The simulation of such a flux with GEANT4 is too CPU intensive. There are three alternatives to estimate the background. With GEANT4 one can simulate smaller tanks of different size and then extrapolate to the background for the full size. Alternatively the fast simulation program mentioned above was used. The third method is based on the peak to Compton ratio and the detection efficiency as measured with a  $^{228}\text{Th}$  source for a similar detector.<sup>2</sup> Then the absorption length of the  $^{208}\text{Tl}$  photon is used to analytically calculate the background index for a given shielding and surface activity.

For example, the shielding of a surface activity of 0.26 Bq/cm<sup>2</sup> from the concrete/rock with 570 cm of liquid nitrogen results in a background index

$$B = 5 \cdot 10^{-3} \frac{\text{cm}^2}{\text{keV} \cdot \text{kg}} 0.26 \frac{1}{\text{cm}^2 \cdot \text{sec}} e^{-570 \cdot 0.03115} = 2.5 \cdot 10^{-11} \frac{\text{cts}}{\text{keV} \cdot \text{kg} \cdot \text{sec}} \quad (6)$$

$$= 0.8 \cdot 10^{-3} \frac{\text{cts}}{\text{keV} \cdot \text{kg} \cdot \text{y}} \quad (7)$$

where  $5 \cdot 10^{-3} \text{cm}^2/(\text{keV} \cdot \text{kg})$  is the measurement result and  $\mu = 0.03115 \text{ cm}^{-1}$  is the absorption coefficient in liquid nitrogen.

All methods predict within a factor of two the same background suppression. Different design options for the tank are discussed in section 5. The resulting background indices are calculated with the above formula.

Note that the detection of scintillation light in LAr could result in a background rejection factor of 20 (see section 3.4). This has not been taken into account in the current design.

### *Neutron induced background*

The main sources of neutrons in the LNGS are from spontaneous fission (dominated by the  $^{238}\text{U}$  isotope) and from  $(\alpha, n)$  reactions in the concrete and the rock. The maximum neutron energy from these processes is about 9 MeV. Neutrons above this energy originate from muon interactions which have a much smaller flux.

No detailed measurements of the neutron energy spectrum exist. Instead the spectral shape is taken from a simulation of the above processes [Wul 03]. The predicted integral flux of  $4 \cdot 10^{-6}$  neutrons/(cm<sup>2</sup>·sec) is in agreement with measurements.<sup>3</sup> The energy spectrum is shown in Fig. 6. The peak in the spectrum at 6.75 MeV is due to  $(\alpha, n)$  reactions on magnesium and carbon. Neutrons above 7 MeV are from fission.

---

<sup>2</sup>The peak to Compton ratio is defined here as the number of events in the 2.615 MeV peak to the number of events in the energy interval of 2.00 - 2.08 MeV.

<sup>3</sup>For a more detailed discussion see [Wul 03] and references therein.

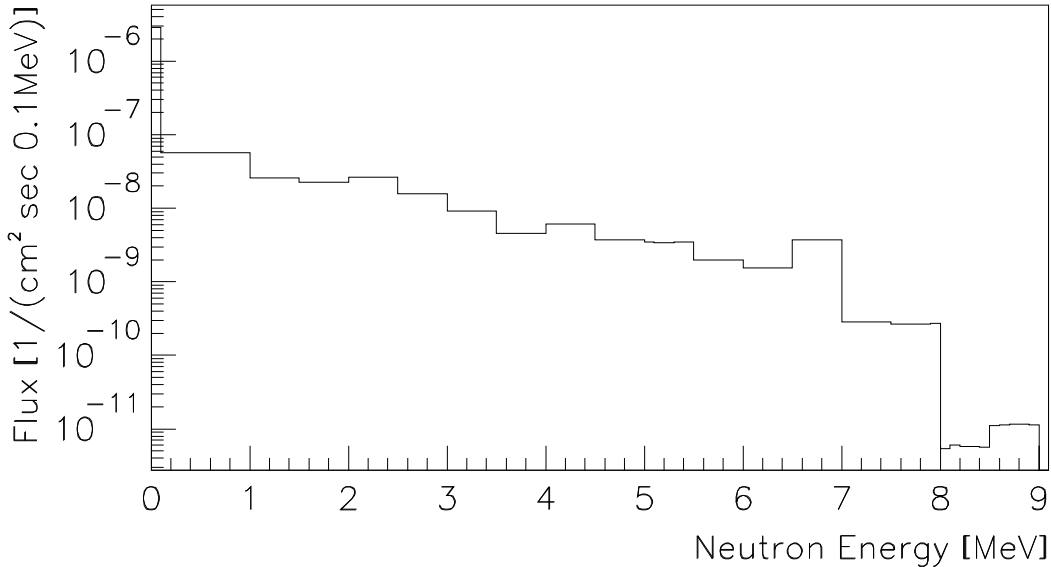


Figure 6: Prediction of the energy spectrum of neutrons in LNGS Hall A from fission and  $(\alpha, n)$  reactions [Wul 03].

A spherical vessel of 7 m diameter plus a variable thickness of polyethylene as a moderator is simulated. The results shown here will not depend on the exact shape of the tank. It should be noted, however, that the simulation assumes hermetic moderator shielding.

The simulation in GEANT4 is based on cross section tables for all the relevant isotopes. Tables are available for elastic scattering, capture  $(n, \gamma)$  and inelastic reactions  $(n, n\gamma)$ ,  $(n, p)$ ,  $(n, p\gamma)$ .

In Table 3 the neutron flux and the mean neutron energy after the polyethylene moderator is given. With increasing thickness more and more slow neutrons are captured, and consequently the spectrum becomes harder. Since nitrogen also acts as an additional moderator, neutron background is more critical for argon filling, and we primarily address this case. In liquid argon neutrons lose typically only a few percent of their energy per elastic scattering and the mean free path is 15-20 cm above a kinetic energy of 0.5 MeV. Consequently most neutrons are backscattered and stopped in the moderator.

A moderator thickness of 40 cm was simulated in detail. In Fig. 7 a) the neutron energy spectrum is shown for those neutrons that pass the moderator and 3 m of liquid argon. Part b) shows the initial energy of the same neutrons. All slower neutrons are captured and only the neutrons with large initial energy reach the germanium diodes. Here elastic scattering dominates again and almost no neutron is captured in the germanium. The Monte Carlo sample size corresponds to twice the integrated flux for one year. No event was observed in the energy region of  $Q_{\beta\beta}$ . Hence a moderator thickness of 30 cm resulting in a factor of 5 higher flux is also sufficient.

Table 3: Relative neutron flux  $\Phi$  and average neutron energy  $E$  after a polyethylene moderator for different moderator thicknesses.

thickness	0 cm	10 cm	20 cm	30 cm	40 cm	50 cm
$\Phi$	1	0.22	0.031	$6 \cdot 10^{-3}$	$1.3 \cdot 10^{-3}$	$3.8 \cdot 10^{-4}$
$E$ [MeV]	0.52	0.61	0.81	0.97	1.09	1.16

For nitrogen the neutron background is even less of a problem, since the energy loss per scattering is almost a factor of 3 larger and the cross sections are typically a factor of 10 larger. Water will provide a similar shielding as polyethylene.

Presently all options include a thick layer of water (>50 cm) as shield. This will ensure that the neutron background is negligible.

#### *Muon induced backgrounds*

The outer area of the tank is rather large. An instrumented layer of water for the detection Cherenkov light from muons is therefore a cost-effective solution for a muon veto. No detailed design or simulation of the efficiency of such a detector is available at the moment.

For the GENIUS project already a 96% efficiency of the veto resulted in a background index of  $2 \cdot 10^{-6}$  cts/(keV·kg·y) [Bau 99], and therefore details of the veto design are not considered critical at this time. This veto will also reject most of the inelastic muon reactions such as the production of secondary neutrons in the lead shield or the LN/LAr.

#### *Background from contaminations of the liquid nitrogen / argon*

The BOREXINO collaboration has measured upper limits for the contamination of their liquid scintillator of less than  $3.5 \cdot 10^{-16}$  g/g for  $^{238}\text{U}$  and less than  $4.4 \cdot 10^{-16}$  g/g for  $^{232}\text{Th}$  [Ali 98]. Similar limits are expected for LN/LAr since they are also produced by fractional distillation. These limits correspond to 32  $^{238}\text{U}$  decays and 11  $^{232}\text{Th}$  decays per  $\text{m}^3$  and year for liquid nitrogen.

Due to heat losses some of the liquid will evaporate and will be lost. An upper limit of  $200 \mu\text{Bq}/\text{m}^3$  for the  $^{222}\text{Rn}$  contamination is assumed for the liquid supply [MPI 03]. This corresponds to 3.2 atoms/ $\text{m}^3$ . During one year,  $200 \text{ m}^3$  will be exchanged (once the entire volume) and thus 640 decays have to be taken into account. Alternatively, if the contamination does not decay with  $T_{1/2} = 3.8 \text{ d}$  but stays constant (due to permanent emanation), 6300 decays/ $\text{m}^3$  have to be taken into account per year. A simulation shows that even this very conservative assumption leads to an upper limit well below  $10^{-3}$  cts/(keV·kg·y). This can be further reduced by anti-coincidence methods and pulse shape analysis.

If the choice of the liquid is argon, then additional background from  $^{42}\text{Ar}$  decays have to be taken into account. The upper limit on the activity from  $^{42}\text{Ar}$  is  $40 \mu\text{Bq}/\text{kg}$  [Ash 03]. A simulation shows that this results in a background of  $4 \cdot 10^{-5}$  cts/(keV·kg·y). Beta decays of  $^{39}\text{Ar}$  have a  $Q$  value of 0.6 MeV and do not contribute to the background for neutrinoless

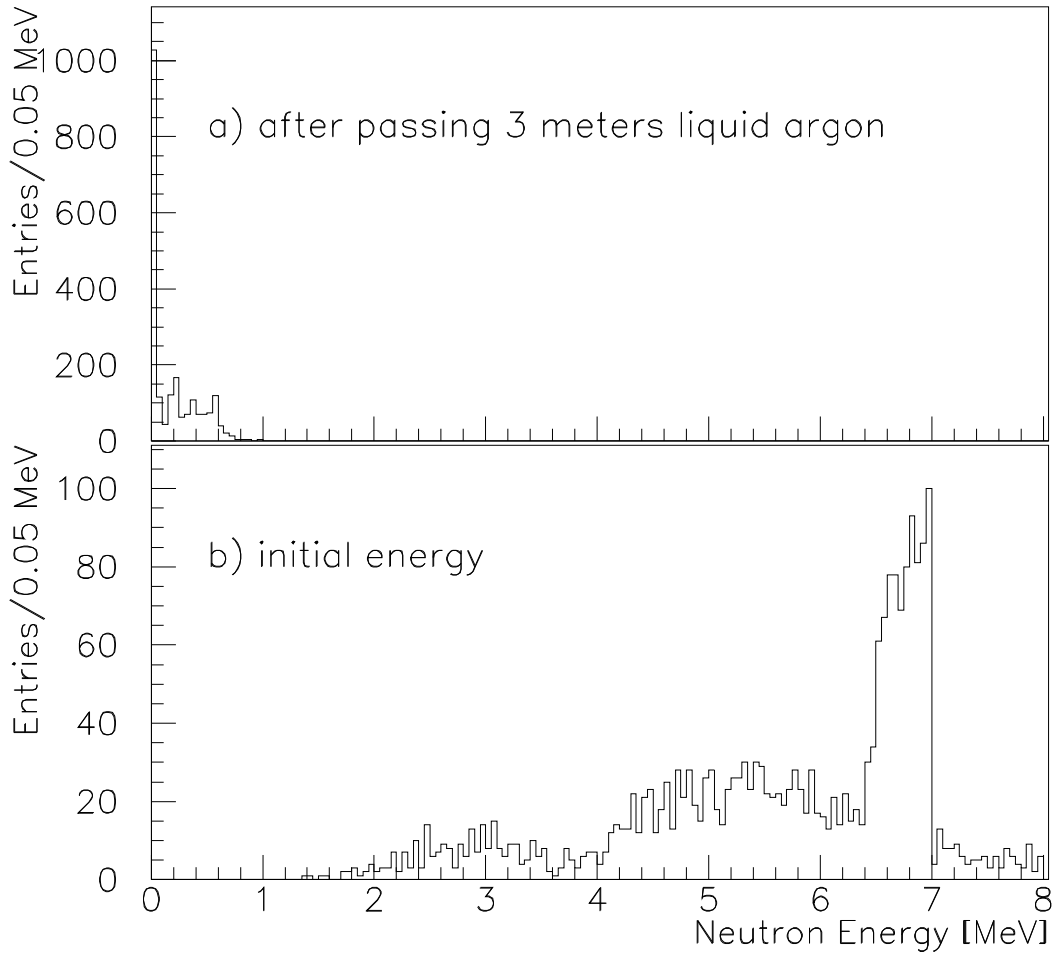


Figure 7: a) Neutron energy after 40 cm of moderator and 3 m of liquid argon. b) Initial energy of these neutrons.

double beta decay.

*Background from the detector surface and the holder material*

The experience of many low background experiments shows that the surface contamination is by far larger than the bulk activity. For coaxial detectors the inner well is critical. To estimate the sensitivity of the experiment to this background,  $^{208}\text{Tl}$  decays were generated at this location. For 2.5% of these decays, the energy deposition is in the interval 2.0-2.08 MeV in one of the crystals (out of 27). About 90% of these events can be rejected by the anti-coincidence with a second detector and an additional factor of 4 can be gained by a 4-fold axial segmentation. Consequently, for a background index of  $10^{-3}$  cts/(keV·kg·y) the surface activity of  $^{208}\text{Tl}$  has to be below  $100 \mu\text{Bq}/\text{m}^2$  without any anti-coincidence method ( $\sim 6$  decays per year and detector) and below  $4 \text{ mBq}/\text{m}^2$  with



the above mentioned rejection factors. The background contribution from  $^{214}\text{Bi}$  decays is about a factor of 10 smaller for the same activities.

For the detectors of the Heidelberg-Moscow experiment there is clear evidence for surface contamination for two of the five detectors [Die 99, Bak 03]. The level is of the order of 45 decays of  $^{210}\text{Pb}$  per year and detector. For the  $^{232}\text{Th}$  decay chain the intensity is approximately a factor of 4 smaller and consequently one would expect about 4  $^{208}\text{Tl}$  decays on the detector surfaces per year. The resulting background index is  $\leq 10^{-3}$  cts/(keV·kg·y). For the other detectors the contamination level of  $^{210}\text{Pb}$  is about a factor of 10 smaller or not seen at all.

Concerning the energy deposition in the crystals and the fraction of events with energy depositions in neighboring diodes or different segments, contaminations in the holder material of the diodes have similar effects as surface contaminations. Therefore for 10 gram holder weights per diode and a background index of  $10^{-3}$  cts/(keV·kg·y), the contamination of the material should be below  $20 \mu\text{Bq/kg}$  of  $^{208}\text{Tl}$  ( $1.5 \cdot 10^{-11}$  g/g of  $^{232}\text{Th}$ ).<sup>4</sup> If the anti-coincidence methods are applied this number can be larger by up to a factor of 40. For the acryl material used by SNO, a contamination level of  $10^{-12}$  g/g for  $^{232}\text{Th}$  was found, resulting in a background index of  $\leq 10^{-4}$  cts/(keV·kg·y).

### 3.3 Background summary

**Phase I:** The external background will be reduced to a level of  $10^{-3}$  cts/(keV·kg·y). From the analysis of the Heidelberg-Moscow data we are confident that the overall background can be reduced by at least a factor of 20 once the diodes with contacts of reduced mass are immersed in LN/LAr (see section 3.1). The background index is then  $\leq 10^{-2}$  cts/(keV·kg·y).

Table 4: Summary of background estimates for Phase II of the experiment. For the assumptions see text. The external  $\gamma$  background is for shielding with LN.

source	background index in $10^{-3}$ cts/(keV·kg·y)
external $\gamma$ from $^{232}\text{Th}$ , $^{228}\text{U}$	1
external neutrons	$\leq 0.05$
external muons	$\leq 0.05$
internal $^{68}\text{Ge}$	0.9
internal $^{60}\text{Co}$	0.1
contamination in LN/LAr ( $^{222}\text{Rn}$ )	$\leq 0.1$
contamination in holder material	$\leq 0.1$
surface contamination	$\leq 0.1$

<sup>4</sup>The background from  $^{214}\text{Bi}$  decays is about a factor of 10 smaller for the same contamination level.

**Phase II:** A summary of the estimated background contributions is given in Table 4. For the estimate of the internal background, realistic assumptions are made for the fabrication times: The time between the enrichment process and the storage underground is 180 days (relevant for  $^{68}\text{Ge}$  production), the time between the last zone refinement and the storage underground is 30 days (relevant for  $^{60}\text{Co}$  production) and the time between the storage underground and the start of the measurement is 180 days (relevant for  $^{68}\text{Ge}$  decay). For the anti-coincidence methods a four-fold axial segmentation and a corner location of the diode in the setup is used. In addition, a factor of two for background rejection is assumed from pulse shape analysis.

### 3.4 Performance with instrumented shield for LAr

The design of our proposal consists of germanium diodes immersed in liquid nitrogen or argon. The liquid serves as a high purity *passive* shield against radiation. Ionizing radiation that creates background signals in the diodes with energies close to  $Q_{\beta\beta}$  typically has energies greater than the one deposited in the germanium crystals. Part of this energy is dissipated in the shielding liquid and is ‘invisible’. An option under study is to instrument the shielding medium and to measure the energy deposition which can be used as an anti-coincidence signal. Liquid nitrogen provides only weak signals from scintillation and Cherenkov light emission. The scintillation properties of liquid argon are well established, see [Kub 79, Dok 90, Hit 83, Cen 99]: about 40,000 photons are emitted per MeV of deposited energy. This is approximately four times the number observed in organic liquid scintillators. Photons are emitted in the de-excitation of the  $\text{Ar}_2^*$  excimer with a wavelength of 128 nm. Decays from singlet and triplet excited states give rise to a fast 6 ns and a slow 1.6  $\mu\text{sec}$  component with an intensity ratio of 0.3 for excitation with electrons, and of 1.3 for alpha particles [Kub 79].

In order to use the scintillation light in anti-coincidence with the germanium diodes, one has to detect the 128 nm scintillation photons with high efficiency. The use of wavelength shifting materials to move the photon wavelength into the region of maximal sensitivity of Bi-alkali photomultipliers is under investigation. Technical details of this developments are summarized in section 7. A Monte-Carlo simulation of a 2 kg diode immersed in liquid argon demonstrates the potential power of the method. We assume that a threshold of 100 keV can be achieved for the detection of scintillation light. Figure 8 displays the results of simulations of  $^{42}\text{K}$  decays, the progeny of  $^{42}\text{Ar}$  ( $Q_{\beta} = 0.6$  MeV,  $t_{1/2} = 33$  y), homogeneously distributed in the liquid argon.  $^{42}\text{K}$  has a maximum electron energy of 3.5 MeV and a weak  $\gamma$  line at 2.424 MeV and thus is a relevant background for double beta decay. A ratio of  $^{42}\text{Ar}/^{nat}\text{Ar}$  of  $3 \cdot 10^{-21}$  has been assumed [Bar 02] for the simulation. A background suppression of more than a factor of 100 is achieved in the  $Q_{\beta\beta}$  region.

Figure 9 shows a simulation of cosmogenic  $^{60}\text{Co}$  decays which are placed homogeneously inside a germanium crystal. An activity of 0.18  $\mu\text{Bq}/\text{kg}$  is assumed. Again, one gains two orders of magnitude in background suppression.

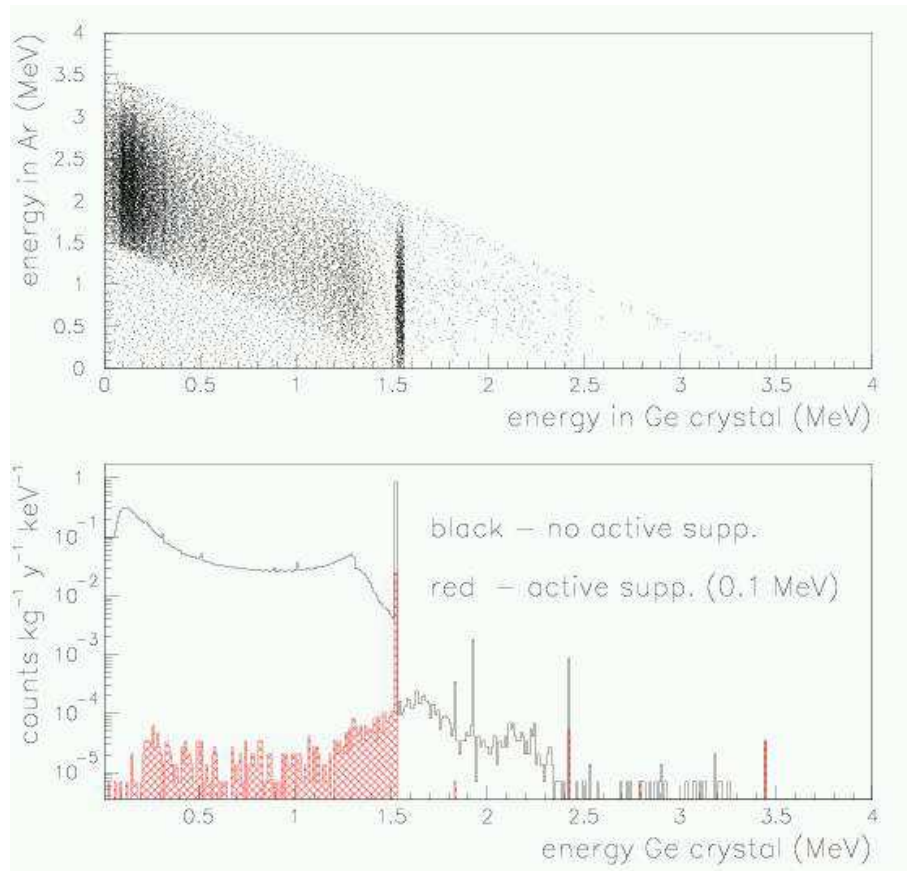


Figure 8: Suppression of external  $^{42}\text{K}$  ( $^{42}\text{Ar}$  progeny): Scatter plot of the energies deposited in the liquid argon and the Ge diode (top), and the energy spectrum seen by the germanium crystal with and without anti-coincidence assuming a threshold of 100 keV (bottom).

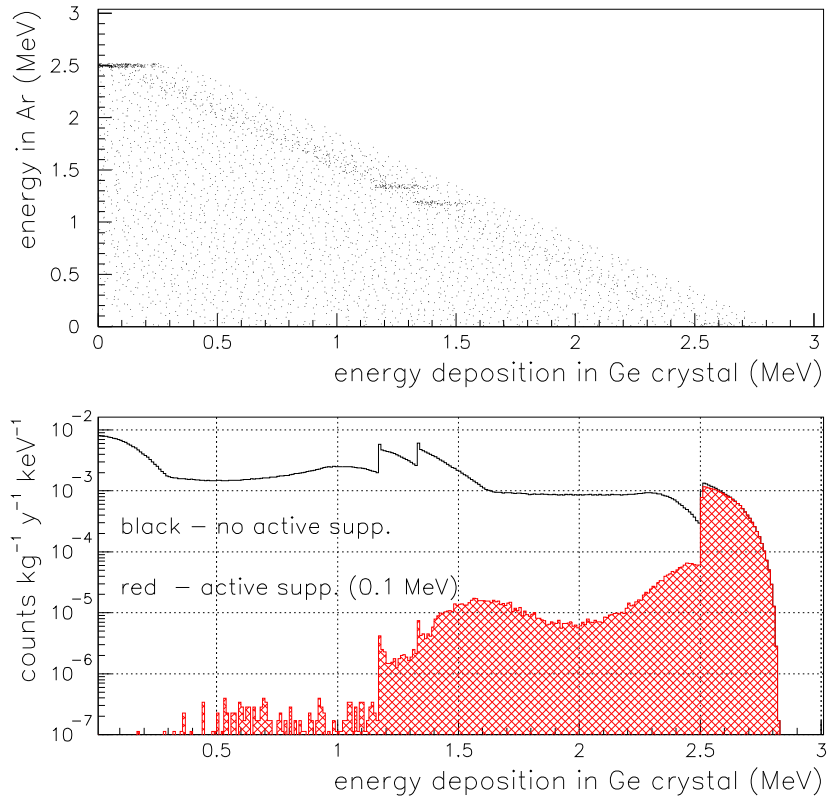


Figure 9: Suppression of internal  $^{60}\text{Co}$  activity: Scatter plot of the energies deposited in the liquid argon and the Ge diode (top), and the energy spectrum seen by the germanium crystal with and without anti-coincidence assuming a threshold of 100 keV (bottom).

## 4 Physics reach

The experiment will have several phases. In the first phase the existing enriched germanium detectors will be used while new diodes need to be fabricated for the second phase. The sensitivities are discussed in the following.

### 4.1 Phase I

For the case that no background events are observed, the 90% confidence limit (C.L.) on the half lifetime for the neutrinoless double beta decay is given by

$$T_{1/2} > 2.4 \cdot 10^{24} \cdot \epsilon \cdot a \cdot M \cdot t \quad [y] \quad (8)$$

with  $\epsilon$  being the detection efficiency,  $a$  being the enrichment fraction of the  $^{76}\text{Ge}$  isotope,  $M$  being the total active mass of the diodes in kilograms and  $t$  being the measurement time in years.

If the number of background events is large and Gaussian errors can be assumed, the same confidence level limit is given by

$$T_{1/2} > 4.3 \cdot 10^{24} \cdot \epsilon \cdot a \sqrt{\frac{M \cdot t}{B \cdot \Delta E}} \quad [y] \quad (9)$$

with  $B$  being the background index in  $\text{cts}/(\text{keV} \cdot \text{kg} \cdot \text{y})$  and  $\Delta E$  being the energy resolution in keV.

For the first phase of the experiment only existing enriched detectors will be used. In total, the active mass of the existing enriched detector is almost 20 kg. Here we will only assume an active mass of 15 kg, since some the detectors might not work reliably.

The reduction of the external backgrounds to a level of less than  $10^{-3}$   $\text{cts}/(\text{keV} \cdot \text{kg} \cdot \text{y})$  is ensured by the design of the tank and the reduction and selection of the detector mounting material. For the intrinsic background we assume a level of  $10^{-2}$   $\text{cts}/(\text{keV} \cdot \text{kg} \cdot \text{y})$  as discussed in section 3.1.

Assuming one year of data taking and a resolution of 3.6 keV, the expected number of background events is 0.5 counts. If no event is observed (60% chance), a 90% C.L. of  $T_{1/2} > 3.0 \cdot 10^{25}$  y can be established for a detection efficiency of  $\sim 95\%$  and an enrichment fraction of 86%. This results in an upper limit on the effective neutrino mass of  $m_\nu < 0.24 - 0.77$  eV. The mass range is determined by the matrix elements quoted in [Ell 02]. If the possibility of a non-zero event count is taken into account (with weights determined by a poison distribution of mean 0.5 events) then the upper limit becomes  $T_{1/2} > 2.2 \cdot 10^{25}$  y or, translated into an effective neutrino mass,  $m_\nu < 0.28 - 0.9$  eV.

The current claim of a signal for neutrinoless double beta decay [Kla 04] is based on an excess of  $28.8 \pm 6.9$  events for a total statistics of 71.7 kg·y. With a statistics of one year data taking of 15 kg·y and a similar detection efficiency we would observe  $6.0 \pm 1.4$  events above a background of 0.5 counts. If no event is observed, the claim would be ruled out with 99.6% confidence level. If one event were observed, it would be a 97.8% confidence

level. However, if six or more events would be observed, this would correspond to a 5 sigma confirmation.

If some of the detectors exhibit a larger background index the same sensitivity can be reached with a subset and a correspondingly larger running time.

## 4.2 Phase II

In the second phase of the experiment new germanium detectors will be added to the setup. A background index of  $10^{-3}$  cts/(keV·kg·y) is achievable, if the detector exposure can be kept to the limits discussed in section 3.3.

It is foreseen to accumulate statistics of about 100 kg·y within 2-3 years. With a resolution of 3.6 keV, 0.36 background counts are expected. Consequently there is a large chance that no event is observed. The limit on  $T_{1/2}$  would improve by a factor of six to  $2 \cdot 10^{26}$  y. This translates to an upper limit of the effective neutrino mass of 0.09 - 0.29 eV, depending on the nuclear matrix element used.

# 5 Technical aspects of the experiment

## 5.1 Overview

Figure 10 shows a schematic of the experimental setup. Via the cleanroom, the Ge diodes are brought via the cleanroom to the lock through which they are installed in the cryogenic vessel filled with either liquid nitrogen (LN) or liquid argon (LAr). The cryofluid serves both as cooling and shielding medium for the diodes. The detector suspension and contacts are made out of a minimum of carefully screened materials of ultra-high radiopurity. The vessel is hermetically enclosed by a passive neutron absorber consisting of water and/or polyethylene. Signals induced by incident muons are rejected with the help of muon detectors - scintillators on top of the vessel and photomultiplier tubes in the water detecting Cherenkov light.

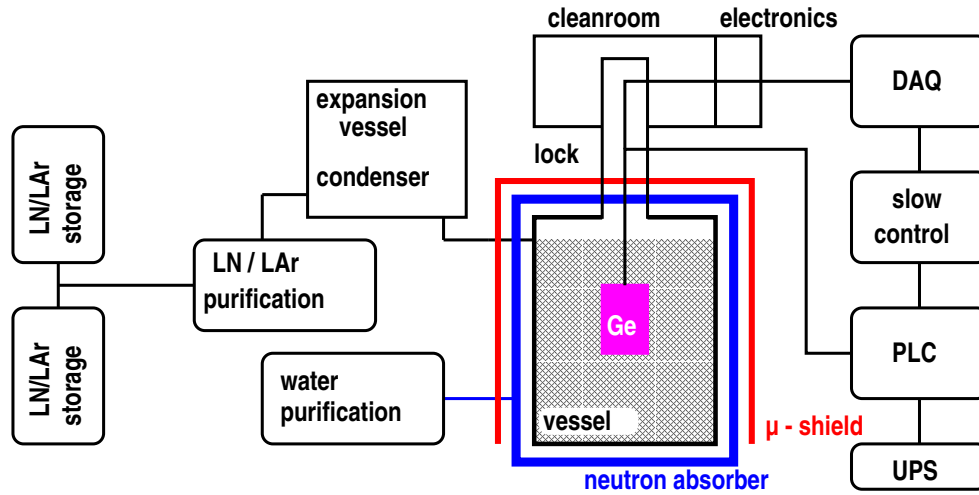


Figure 10: Schematic of the experimental setup. Part of the muon shield is integrated in a water tank serving both as shield against  $\gamma$  background and neutron absorber.

The signals of the Ge diodes are led via feed-throughs into the electronic cabin on top of the vessel where their pulse shapes are digitized in flash ADCs. The PC based data acquisition system allows the processing, visualization, quality control, and storage of the incoming data. The slow control supervises all auxiliary systems including the low and high voltage power supplies and the monitoring of the parameters characterizing the status of the experiment like temperature, pressure, detector currents, etc. The programmable logic controller (PLC) is an autonomous system of high reliability for the monitoring of safety relevant parameters like vessel pressure, oxygen concentration, and temperature. An uninterruptible power supply (UPS) allows the system to continue data taking or to reach a safe state in case of an electrical power outage.

The cryogenic vessel is sealed with metal gaskets and operated at 0.2 bar overpressure to prevent contamination of the cryofluid by radon from the environment. It might be

necessary to purge the cryofluid continuously from Rn contamination. This is done by low temperature charcoal adsorber columns which are used also to supply fresh Rn free cryofluid as substitution for evaporated LN/LAr. In case of LAr it might be, however, more economic to re-condense the LAr vapor with either a cryogenerator or an over-pressurized LN radiator coil. Preferentially, both devices would be installed in a small expansion vessel that will allow also to fill the cryogenic vessel up to the edge. Purification of the shielding water is needed to establish sufficient transparency for the detection of Cherenkov light; the radiopurity should be less than that of the construction materials, stainless steel and insulation.

In the following section we will discuss some of the components in more detail and outline planned R&D activities.

## 5.2 Cryogenic tank options

The generic design of the vessel is discussed within two limits requiring that the activity of the surrounding concrete (10 Bq/kg  $^{228}\text{Th}$ ) has to be suppressed by either a factor of  $2.4 \cdot 10^{-9}$  or  $2.4 \cdot 10^{-8}$ . This will yield in the Ge energy spectrum between 2.00 and 2.08 MeV a background of  $10^{-4}$  resp.  $10^{-3}$  cts/(keV·kg·y), i.e. more than 3 resp. 2 orders of magnitude better than achieved in the Heidelberg-Moscow and IGEX experiments ( $\sim 0.2$  cts/(keV·kg·y)).

Table 5: Linear absorption coefficients  $\mu$  for 2.6 MeV  $\gamma$  rays in various materials and the material's intrinsic  $^{228}\text{Th}$  activities assumed in the present discussion.

material	$\mu$ [ $\text{cm}^{-1}$ ]	activity [ $\mu\text{Bq/kg } ^{228}\text{Th}$ ]
LN	0.03115	
Water	0.0427	7000
LAr	0.05	
Steel	0.299	7000
Pb	0.484	30

The vessel dimensions are constraint by the available space in Hall A of the LNGS to a diameter of 12 m and an effective height of 11 m. This space includes the volume needed for the neutron moderator and the  $\mu$  veto system. This leaves a height of about 2.5 m on top of the vessel which is needed for the lock and cleanroom through which the Ge detectors can be installed in the vessel.

Cost and size of the vessel depend significantly on the choice of insulation. Most efficient would be the use of superinsulation which at thermal losses of about  $2 \text{ mW/m}^2\text{K}$  needs marginal space, typically less than 20 cm. Its implementation requires a special double-walled container which is able to maintain a vacuum of better than  $10^{-3}$  Pa between both shells. The more cost effective alternative is to take a normal flat bottom tank as proposed for GENIUS [Kla 99]. This device has a standard powder (perlite) insulation, which due to



its much higher thermal conductivity ( $\sim 40$  mW/Km) needs to be much thicker, typically 1 m.

Last not least, the vessel dimensions depend crucially on the choice of the shielding (and cooling) medium. If LAr would be used instead of LN, the dimensions could shrink by the inverse ratio of their densities, i.e. by a factor of 0.62, (see Tables 5 and 6) and there would be, in fact, no problem to fit a LAr container in Hall A. Since we prefer to keep

Table 6: Thickness of various absorber materials needed to achieve the indicated background levels at indicated activities of steel and lead.

	thickness [cm] for $10^{-3}$ [cts/(keV·kg·y)]	thickness [cm] for $10^{-4}$ [cts/(keV·kg·y)]
shield against concrete of 10 Bq $^{228}\text{Th}/\text{kg}$		
1 LN	563	637
2 LAr	350	396
3 Fe	58.6	66.3
4 Pb	36.2	41.0
shield against steel of 7 mBq $^{228}\text{Th}/\text{kg}$ (3.34 cm = 1/e)		
5 LN	330	404
6 LAr	205	251
7 Pb	21.2	26.0
shield against steel and concrete (liquid - steel - Pb - concrete)		
8 LN + Pb	330+12.9	404+12.9
9 LAr + Pb	205+12.9	251+12.9
shield against Pb of 30 $\mu\text{Bq}$ $^{228}\text{Th}/\text{kg}$ (2.07 cm = 1/e)		
10 LN	151	225
11 LAr	94	140
shield against Pb, steel, concrete (liquid - Pb - steel - concrete)		
12 LN + Pb	151+24.4	225+24.4
13 LAr + Pb	94+24.4	140+24.4

both options, we will discuss here optimized solutions which allow either the use of LN or LAr in an affordable way. For this purpose, we consider just those tank options which will provide with LN a background level of  $10^{-3}$  cts/(keV·kg·y) and reach  $10^{-4}$  cts/(keV·kg·y) with a LAr fill only.

### 5.2.1 Superinsulated vessel

The realization of the original idea [Heu 95] to use exclusively purified liquid nitrogen as shielding material implies a LN thickness of 6.4 (5.6) m for arriving at the desired background level of  $10^{-4}$ ( $10^{-3}$ ) cts/(keV·kg·y), see Table 6. A detailed study [Bab 03] has

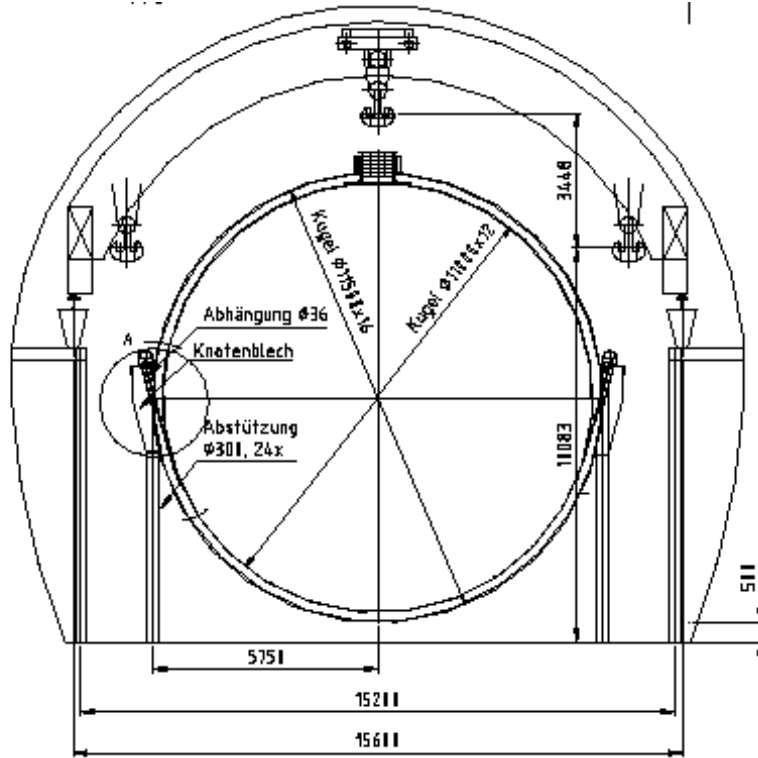


Figure 11: A vacuum insulated spherical LN vessel with an inner diameter of 11 m in Hall A of LNGS.

shown that it is possible to realize a vacuum insulated sphere with an inner diameter of 11 m (or a lying cylinder of 11 m diameter and 12 m length) that would fit into Hall A of LNGS (see Fig. 11) and exhibit the structural stability needed to withstand an earth quake with an acceleration of 0.3 g. If the LN would be substituted by LAr, the dimensions would shrink to a diameter of 8 (7) m for a background of  $10^{-4}$ ( $10^{-3}$ ) cts/(keV·kg·y). However, this solution turned out to be prohibitively expensive, even disregarding the problem caused by the marginal space available for the neutron shield.

The GEM project [Zde 01] - a LN filled superinsulated copper sphere of 5 m diameter suspended in a water basin of 11 m diameter - fits also in the category of superinsulated vessels. It is not discussed here since the technical realization seems to be more difficult and expensive than a similar design described below.

### 5.2.2 Flat bottom tank

The design of a flat bottom tank of the required shielding power with both LAr and LN fills has to combine conventional and LN/LAr shields in order to fit into the available space. Table 5 lists the linear absorption coefficients for 2.6 MeV  $\gamma$ - rays in LN and LAr as well as in steel, lead and water. Accordingly, 6.44 cm of lead or 72.9 cm of water can

substitute a 1 m thick LN layer. Water is an attractive substitute not only because it is cheap but also since it can serve simultaneously as neutron absorber and Cherenkov medium for the detection of muons. In arranging the different materials, an additional constraint, however, is the radiopurity of the involved materials. Activities of 7000 resp.  $30 \mu\text{Bq } ^{228}\text{Th}/\text{kg}$  have been measured for the steel used in the LENS experiment and for commercially available lead, respectively, and we adopt these values for the further discussion. In this context, Fig. 12 serves to illustrate typical features of a commercially available [Cmp 04] flat bottom vessel; almost no modifications were made to account for

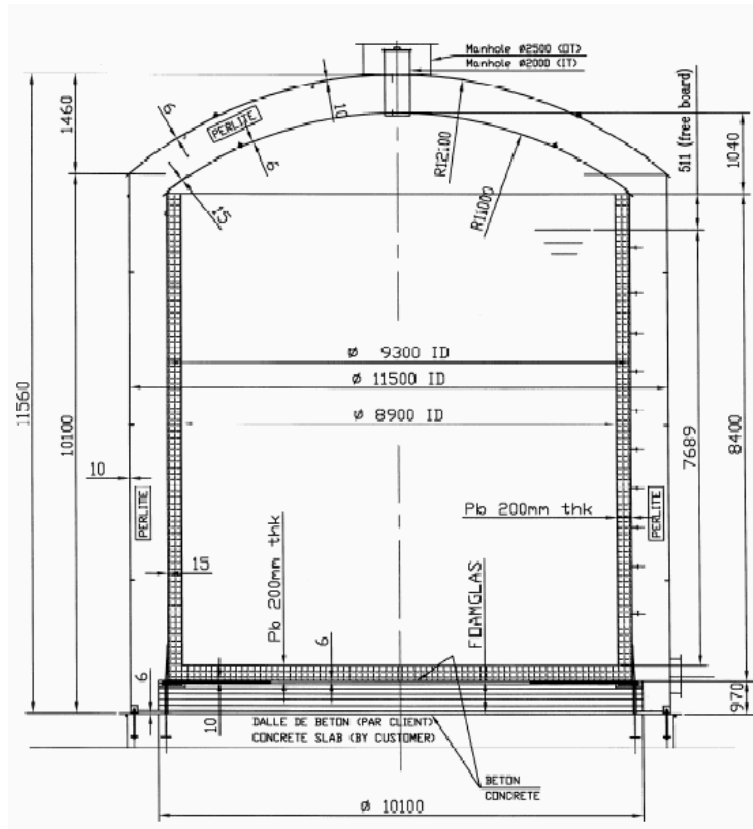


Figure 12: Cross section of a commercial flat bottom vessel for  $473 \text{ m}^3$  LN or LAr with slight modifications to carry a non-standard internal Pb shield (design by CMP Arles [Cmp 04]).

the load by the non-standard internal Pb wall. The vessel's base plate is bolted onto 1 m high concrete slabs supplied by the customer; (thus the vessel shown is  $\sim 1$  m too high to fit into Hall A). The  $\sim 1$  m thick insulation between the base plate and the inner vessel bottom consists of foam glass sandwiched between two 8 cm thick concrete layers. The remaining insulation is provided by a 1.1 m thick perlite layer. Table 7 shows measured  $^{228}\text{Th}$  activities for various insulation materials. Since foam glass exhibits the same activity as the LNGS concrete, there is no other choice but to install a lead shield together with

Table 7: Comparison of various isolation materials. The symbols  $A$ ,  $\lambda$ ,  $\rho$ , and  $\xi$  denote the  $^{228}\text{Th}(\text{Th})$  radioactivity, thermal conductivity, density and compressive strength, respectively. Class refers to German or British fire prevention classes.

material	A	$\lambda$	$\rho$	$\xi$	class
	$[\mu\text{B}/\text{kg}]$	$[\text{mW} / \text{Km}]$	$[\text{kg}/\text{m}^3]$	$[\text{kg}/\text{mm}^2]$	
Perlite	$3.5 \cdot 10^7$	45 - 70			A1
Foam glass	$1.0 \cdot 10^7$	40 - 60			A1
Polystyrol (EPS)	2100	30 - 40	15 - 30		B1
Styrodur C <sup>a</sup>		40	25 - 45	200 - 700	B1
Elastopor <sup>b</sup>	d)	33.5		0.4	B3
Ecopir <sup>b</sup>			33		
Ecophen <sup>c</sup>		18	60 - 160		0

<sup>a</sup> Polystyrol

<sup>b</sup> polyisocyanurate/polyurethane rigid foam

<sup>c</sup> phenolic foam

<sup>d</sup> measurements in progress

the neutron absorber above the foam glass-concrete insulation, i.e. at the bottom of the cold volume. Table 7 shows in addition that at 30 Bq/kg the activity of perlite is even higher than that of the LNGS concrete (10 Bq/kg). This rules out the use of this material. A substitute with even lower thermal conductivity is polystyrol. Further candidates are polyisocyanurate and phenolic rigid foams. Measurements are in progress to determine their activities. For the present purpose, the activity of the insulation is assumed to be equal or less than that of the steel.

Based on the above considerations and constraints, two natural options for the layout of a flat bottom cryogenic vessel emerge, and Table 6 compiles the data for these options, assuming (A) installation of the lead mostly outside the vessel or (B) completely within the cryofluid. It is assumed that the Ge detector assembly has a cylindrical shape of 50 cm diameter and 50 cm height, and that the insulation has a thickness of 1.1 m. If not mentioned explicitly, the radiopurities of steel, lead, and water are those listed in Table 5.

**Option A.** The first alternative assumes standard commercial insulation at the bottom of the vessel, i.e. foam glass and concrete, and a lateral insulation with an activity that is lower or equal to that of steel (7 mBq/kg  $^{228}\text{Th}$ ). The resulting vessel layout is shown at the right hand side of Fig. 13. Laterally and on top, the lead is placed outside the vessel. The minimum thickness of the cryofluid results from the constraint that it reduces the background caused by the steel walls and the insulation to the desired level. For a background level of  $10^{-3}$  cts/(keV·kg·y) a thickness of 330 cm is needed for LN. With LAr this thickness is more than enough to reach a level of  $10^{-4}$  cts/(keV·kg·y) (see lines (8) and (9) in Table 6). The thickness of the additional lead needed to reduce also the radiation from the surrounding concrete to the desired level is 12.9 cm. As discussed above, the high

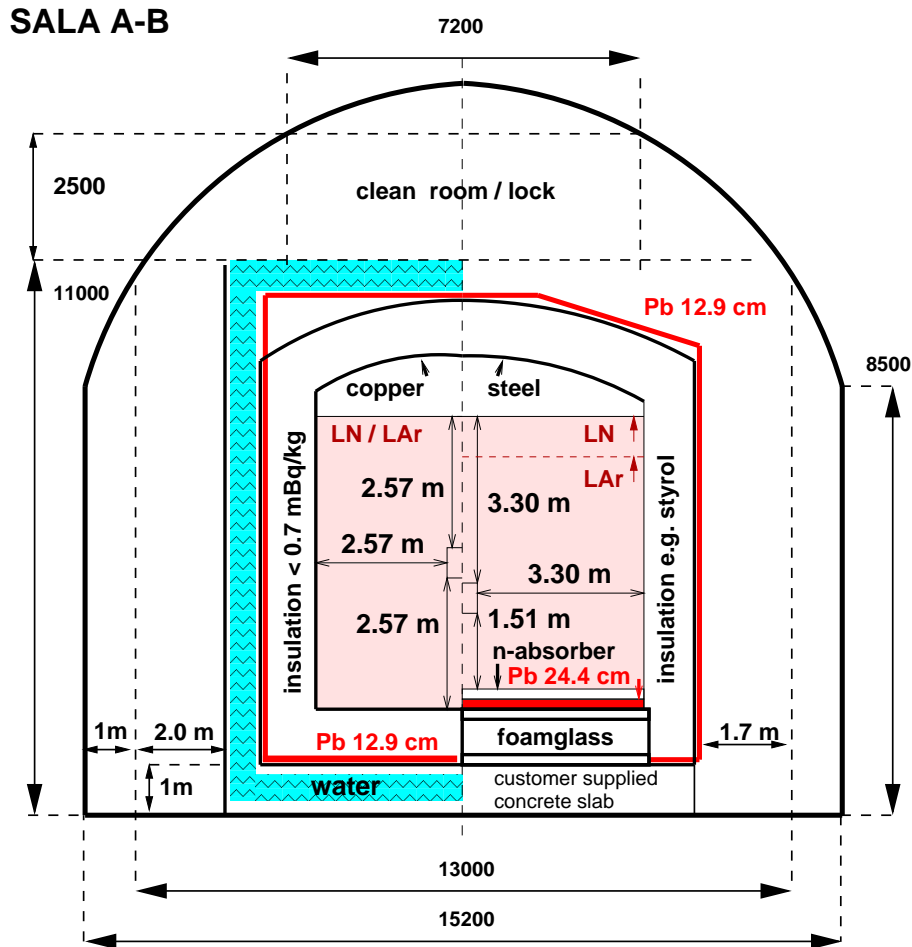


Figure 13: Possible layouts, options A (r.h.s.) and A' (l.h.s.), for a cryogenic vessel fitting into Hall A. The outer contour shows the cross section of Hall A.

radioactivity of the foam glass at the bottom enforces the lead shield to be placed here in the cold volume together with the neutron absorber, e.g. a 30 cm thick polyethylene panel, placed on top of it. The diameter and effective height of the vessel are about 10 m and 11 m, respectively. These dimensions would allow one to replace part of the lateral lead shield by water. With LAr, the vessel would not need to be completely filled in order to yield a background index of  $10^{-4}$  cts/(keV·kg·y).

**Option A'.** If materials of lower radioactivity were available, a much more satisfactory layout would be possible as shown at the left hand side of Fig. 13. The idea is to find a rigid foam of less than  $700 \mu\text{Bq/kg}$   $^{228}\text{Th}$  which would provide enough structural strength to allow for a thin inner vessel wall made of copper or low-activity stainless steel. Rigid foams of suitable strength and thermal conductivity are indeed on the market - the still open question is their radiopurity. Relative to option A the LN thickness can be reduced further by 73 cm, the lead can be placed on the warm side of the insulation volume just in

front of the outer steel wall, and the remaining shielding power can be provided by a layer of water whose thickness (40 cm) is equivalent to the 73 cm of LN. Obviously this layer requires no extra space but a third wall.

**Option B.** This alternative leads to a most compact cryogenic vessel as shown Fig 14 (see also Fig. 2). Starting point is the configuration of line (12) in Table 6 with the lead inside

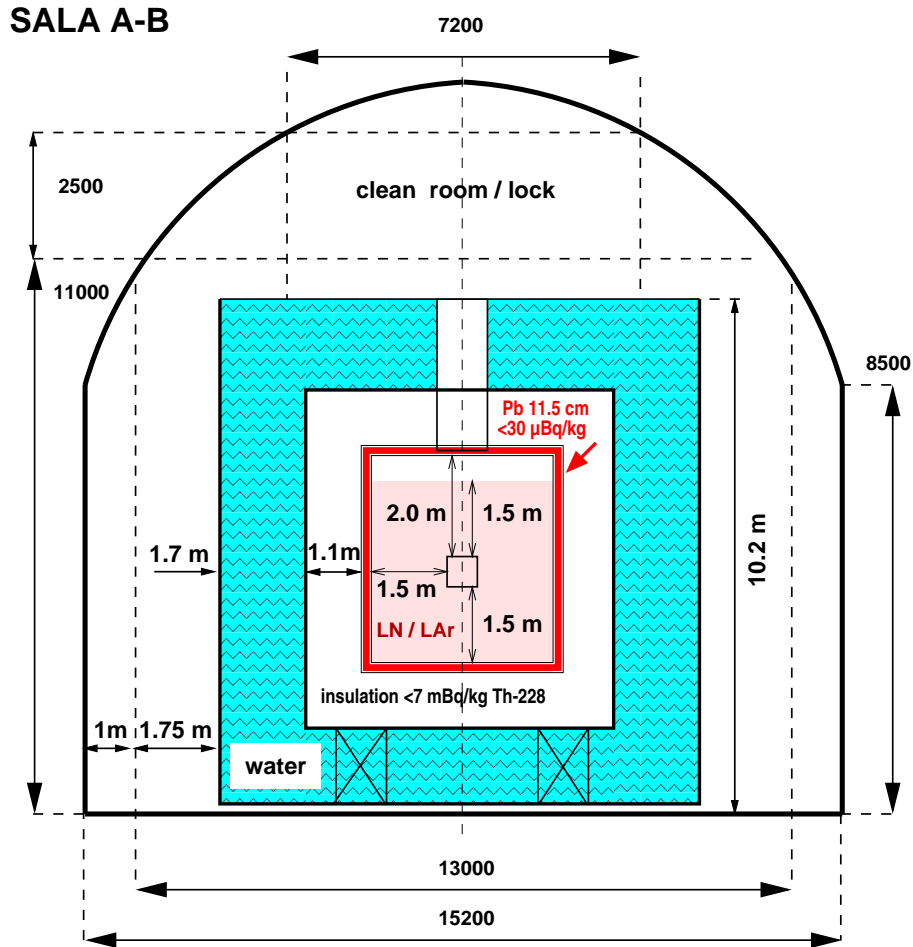


Figure 14: Alternative layout for a cryogenic vessel fitting into Hall A: the option B. The outer contour shows the cross section of Hall A.

the cryofluid immediately in front of the inner wall. Studies of a specialized commercial company show the feasibility of this concept. The lead wall can be stacked such that it is self-supporting and exhibits the required stability against earthquakes [JLG 04].

To shield the lead of  $30 \mu\text{Bq/kg}$   $^{228}\text{Th}$  activity, a LN thickness of 151 cm is needed for a background level of  $10^{-3}$  cts/(keV·kg·y). The thickness of additional lead required to reduce also the radiation from the surrounding concrete to the desired level is 24.4 cm. For obvious reasons, one would choose the lead thickness in the cold volume as small as possible, 11.5 cm, to shield the activity of the steel wall and the insulation. The remaining

12.9 cm could be mounted outside the cold volume or, in view of the largely reduced overall dimensions, substituted by a 171 cm thick water layer. The obvious savings in space and price might be even larger if the insulation thickness can be cut roughly in half: with a total diameter of less than 5 m, the cryogenic vessel could be manufactured at a company and transported as a unit to LNGS. The reduction of insulation thickness could be realized with evacuated powder insulation being standard for tankers, or with superinsulation. In fact, a Russian company offers at a competitive price a standard superinsulated vessel with an inner diameter of 3 m and suitable height between 4 and 6 m. In case of a superinsulated vessel made out of copper of  $\leq 30 \mu\text{Bq/kg}$   $^{228}\text{Th}$  the lead could even be placed outside the cold volume.

### 5.2.3 Conclusions

Despite the many attractive features, superinsulated vessels show - with the exception discussed above - for the intended use no real advantage when compared to flat bottom tanks; they are not only more expensive but also not so flexible if instrumentation of the LAr is considered. For this purpose, an upright cylindrical flat bottom vessel with well distributed locks in the roof is close to the ideal solution.

If one would discard the LN option in exclusive favor of LAr, a conventional flat bottom vessel of 10 m diameter, see line (2) of Table 6, with little lead shielding at the bottom would be suitable. Part of the LAr could be even replaced by a water layer for neutron moderation and  $\mu$  vetoing. When filled with LN however, this vessel would yield only a background level of order 0.2 cts/(keV·kg·y), i.e. the level of the Heidelberg-Moscow experiment.

If both the LN and LAr options are to be kept, several alternatives exist depending on the radioactive purity of the insulation materials. Table 8 gives a summary of the options discussed above as well as the requested radiopurity of employed materials. Compared to GENIUS, all options do not only need less space but exhibit a largely reduced volume of cryofluid. Options A' and B, in particular, integrate with a water shield also the neutron absorber in a space-saving way into the layout. In many respects, option B appears most attractive, also from the safety point of view. It uses the lowest amount of lead which is 'cold', however. Apart from a realistic costing which can be established only in close contact with industry, it is essential for the final decision to know if the close distance between lead wall and Ge array has any detrimental effect upon the neutron flux at the detectors.

LVD needs a passage for a tank carrier that is about 2.2 m wide and 6.2 m long. This constraint will be taken into account by placing the LN/LAr vessel slightly asymmetric into Hall A.

## 5.3 Detector suspension

The detectors will be integrated in assemblies allowing for precise relative positioning and modular insertion. The construction is to minimize material while using only low activity

Table 8: Characteristics of three cryogenic vessel layouts; for indicated options see also Figs. 13 and 14.

Item		Option			
		A	A'	B	GENIUS/GEM
$\emptyset \times H$	[m <sup>2</sup> ]	10 × 11	9 × 11	10 × 10	14 × 19/11 × 11
LN/LAr volume	[m <sup>3</sup> ]	210 / 178	141	34	1250/50
Mass of Lead	[ton]	~550	~500	98	0/0
Volume of water	[m <sup>3</sup> ]	-	~145	~500	0/1000
<b>Required radiopurities:</b>					
inner wall		7	0.7	7	[mBq/kg <sup>228</sup> Th]
insulation		7	0.7	7	
foam glass		10000	-	-	
outer wall		7	7	7	
lead at bottom		0.03	0.7	0.03	
lead elsewhere		7	0.7	0.03	
water		-	7	7	

materials. The complete system has to hold up to 50 detectors, each with a mass of approximately 2kg. Not all detector crystals will have the same dimensions. This will require special measures to fix the relative positioning. The electrical cables have to be guided in the system. The left picture in Fig 15 shows a possible arrangement of detectors into an inner and outer tier. The hexagonal arrangement minimizes the gaps between detectors. The 7 detectors in a layer of the inner tier have a total mass of about 14 kg. The 12 detectors in the outer tier add 24 kg. Three complete layers would contain 112 kg of germanium.

There are several possibilities to divide the assembly into modules that can be installed and exchanged separately. Individual “vertical strings” are conceivable as well as complete inner and outer tier assemblies that can be installed independently. A cage like construction would guarantee a well defined positioning of the individual diodes as well as an easy exchange; however, it is not clear if such a solution can be realized with the required minimum of material.

## 5.4 Lock and cleanroom

On top of the vessel a cleanroom at slight overpressure with an integrated lock provides the possibility to insert and withdraw detectors in a modular way without contaminating the vessel’s contents. To keep cable lengths short, the frontend electronics, power supplies and the PCs for data acquisition and slow control are placed in a directly adjacent neighbored cabin. Fig. 16 shows a possible floor plan that includes another cabin for the on-site



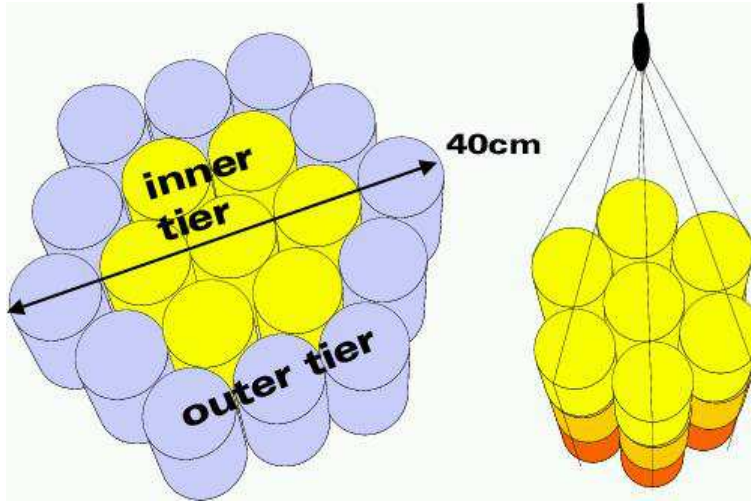


Figure 15: The detectors are arranged into a hexagonal structure. The inner tier contains 7, the outer 12 detectors. The picture on the left shows one complete layer with inner and outer tier. The one on the right depicts three layers of the inner tier with some suspension cables.

control room.

The cleanroom is used for the final preparation of the detectors and their integration into a modular detector suspension system. The detector assemblies are transferred into the main lock through a cleaning pre-lock where they are taken up by a rail system. After the final cleaning procedure the assemblies can only be handled through glove boxes integrated into the main lock. Cables and connectors will be adjusted to that.

The main lock will be operated with a gas atmosphere that is as pure as the vessel gas. In order to prevent radon contamination the glove boxes will be sealed when not in operation. The goal is to keep the lock as clean as possible. However, during data taking the hatch between lock and vessel will be UHV sealed to prevent any long term contamination.

The main hatch will be 80 cm in diameter. The thermally insulated flange will hold the mechanical suspension system and the electrical feed-throughs for high voltage, power supply and signal cables. An additional lead cover will provide shielding in the hatch region.

## 5.5 Neutron and muon shield

The cryogenic vessel is encased by a water layer with at least 40 cm thickness. Its purpose is threefold: (i) to moderate and absorb neutrons, (ii) to attenuate the  $\gamma$  flux, and (iii) to serve as Cherenkov medium for the detection of muons crossing the lateral wall of the experiment. The latter task implies the water to be purified (see subsection 5.9) to assure best transmission of the Cherenkov light. The attenuation length of light should be larger

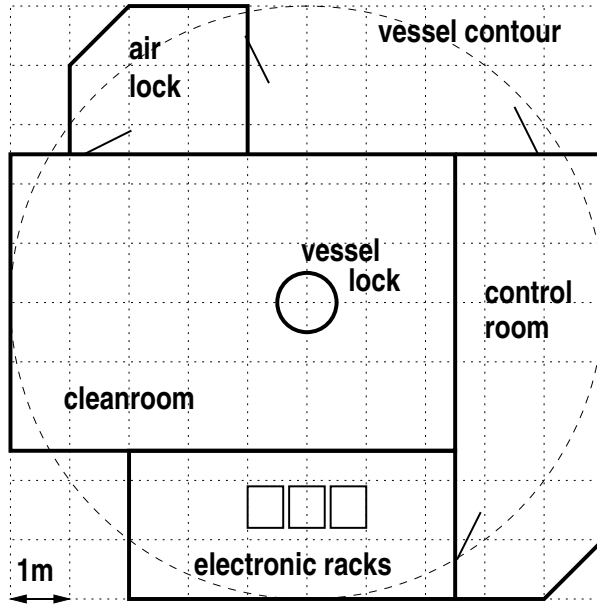


Figure 16: A possible plan of the facilities on top of the vessel including vessel interlock, clean room, electronic hut and on-site control room.

than 10 m at  $\sim 400$  nm wavelength. To maintain high transmittivity and radiopurity the water vessel has to be air tight.

The Cherenkov light is detected by photomultiplier tubes (PMTs), for example the 8" Hamamatsu R1408 PMT that in case of Super-Kamiokande [SuK 03] is covered with a wave length shifter plate of  $60 \text{ cm}^2$  area. Another effective means to increase the number of detectable photoelectrons is to increase the reflectivity of the walls of the water tank. It has been shown, see e.g. [Sho 99], that a lining with Tyvek, a fibrous polyolefin manufactured by Dupont, provides a diffusively reflective surface with greater than 90% reflectivity at the relevant wave lengths around 350 nm.

Since the detailed geometry of the water tank is not yet determined it is not possible to discuss the arrangement of the PMTs in detail. Monte Carlo simulations will be used to study the muon detection efficiency as a function of number and arrangement of the PMTs. A first estimate shows that about 150 PMTs will be necessary to detect muons with sufficient efficiency. These PMTs could be encapsulated together with their remote controlled HV converters, amplifiers and discriminators in watertight acrylic spheres of 12 inch diameter. Strings of such optical modules would be hung down from the top of the water vessel. The PMTs will be working in the single photo-electron regime, and their dark current will imply a counting rate of 10 kHz. Hence a 4-fold 10 ns wide coincidence between neighbored optical modules will be used to identify the signal of an incident muon. The calibration system will consist of a pulsed UV laser whose output is coupled by optical fibers to the individual PMTs.

Of primary importance is the coverage of the top of the vessel. For performance and

logistic reasons, it might here be desirable to choose, instead of water, two layers of scintillator plates which are operated in coincidence.

## 5.6 Electronic readout

Figure 17 shows a schematic of the readout chain for one Ge diode. For optimum noise and speed the input FET of the charge integrating preamplifier is placed close to the detector within the cryofluid. The pre-amplified signal is sampled by a flash ADC (FADC); two such units of high and low gain may be needed if the dynamic range of one unit is not sufficient. Further signal processing including filtering will be done fully digital by digital signal processors (DSPs), field programmable gate arrays (FPGAs) or standard PCs. Algorithms for the real time digital synthesis of pulse shapes have been established [Jor 94, Jor 03] for

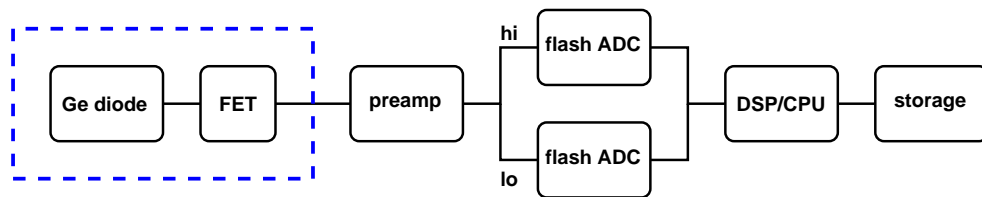


Figure 17: Schematics of the electronic readout chain.

deriving the optimum information on energy and time from a given signal.

Besides the readily available and well proven commercial products for FET and preamplifier, the developments for  $\gamma$  ray tracking detectors like AGATA [AGA] have resulted in frontend electronics optimized for pulse shape analysis with segmented Ge detectors. Besides discrete hybrid solutions also fully integrated ASIC designs are pursued [Del 03]. Typical specifications include a noise level of 1 keV FWHM, a bandwidth of 20 to 30 MHz, a dynamic range of 1000, and a FET power of less than 25 mW which makes these frontends extremely interesting also for the present application.

For the pulse shape sampling and digital signal processing units, several options are available. The commercial fully digital spectroscopy modules of XIA's DGF4C series [XIA] have been chosen as a reference by the MAJORANA collaboration [Maj 03]. The CAMAC based DGF-4C as well as the DGF Pixie-4 module in the CompactPCI/PXI standard provide digital spectrometry and waveform acquisition for four input signals per module with the possibility to combine several modules into a larger system. In the Pixie-4 the signals are digitized in a 14 bit FADC at 75 MHz. Triggering, filtering and time-stamping of the data stream is done in real time in a field programmable gate array (FPGA), and the resulting data can be read out by a computer at up to 109 MB/s. An alternative more cost-effective solution is represented by the GRT4 VME pulse processing card which has been developed for the determination of position, energy and time of an  $\gamma$  event in a segmented Ge detector [Laz 03]. Each of its four channels has a 40 MHz low pass filter including an optional differentiation stage followed by a 14 bit 80 MHz FADC. The VHDL

hardware language is used to implement the desired algorithms in the FPGA. An in-beam test with a 33% efficient Ge detector has shown that the energy resolution is the same as with conventional analog electronics. A third even more cost-effective solution [Kih 03] uses the 8-channel SIS3300 VME FADC module with 100 MHz sampling rate at 12 bit precision. The module is self-triggering and has two memory banks which allow data transfers at 7 MB/s. A low noise amplifier in front of the FADC is used to adjust gain and dc offset. All digital signal processing including pulse shape analysis, integration and pole/zero cancellation was done by a VME CPU with an Intel p3/850 MHz processor running a Linux operating system. This system showed a similar energy resolution as an analog system at a maximum count rate of 4000 events/s and has been installed in the GENIUS test facility at LNGS [Kla 03a].

In conclusion, various attractive readout systems are existing or are becoming available. The final choice will be made after extensive tests and a detailed cost/performance evaluation.

## 5.7 Data acquisition and Slow Control

The data acquisition system will gather the data of the Ge diodes and of the muon counters, and store them with a time stamp on tape. Neither channel count nor acquisition rate will represent a problem - even the muon count rate is only several  $10^{-4}$  events per ( $m^2s$ ). The major requirement will be rather the highest possible operational availability and stability.

The slow control system handles traditionally the non-time critical tasks. It transfers the whole detector system from the safe stand-by mode into the running state (or vice versa) by activating the low voltage power supplies and setting the high voltages for the photomultipliers and Ge-diodes. Concurrently it is reading at typically a few Hertz the various system parameters, and stores any changes of their values with a time stamp in a data base for later retrieval. It also provides a graphical user interface for a breakdown of the status of the various subcomponents, as well as for loading experiment configuration files. Typical system parameters include

- from the vessel: pressure, temperature, gauge of cryogenic fluid and water,
- from the detectors: leakage currents and base currents of the photomultiplier tubes,
- from the electronics: power supply voltages and currents, status of crates, temperatures,
- from the cleanroom: air pressure, oxygen level, radon level, particle concentration,
- from the environment: barometric pressure, humidity, temperature, oxygen level, status of smoke detectors.

If safety relevant alarm conditions are detected, they are immediately communicated to the programmable logic controller (PLC) which forwards them to the LNGS general safety monitoring system. For most safety critical parameters, however, the detour via slow

control is avoided and the monitoring hardware will send its alarm signals directly to the PLC.

The full computerization of the data acquisition and slow control system will allow the sharing of acquired data among all collaboration members practically in real-time, as well as the reliable remote monitoring and control of the whole experiment.

## 5.8 Liquid gas purification

Liquid nitrogen (LN) and liquid argon (LAr) are produced by air separation and thus contain traces of atmospheric noble gases. The most abundant radioactive noble gas nuclides in the atmosphere are  $^{39}\text{Ar}$ ,  $^{85}\text{Kr}$  and  $^{222}\text{Rn}$  (see Table 9).  $^{39}\text{Ar}$  and  $^{85}\text{Kr}$  have Q-values below 700 keV and cannot contribute to the background in the  $0\nu\beta\beta$ -region.

Table 9: The most abundant radioactive noble gas nuclides in the atmosphere (all gas volumes are given at STP).

	$^{39}\text{Ar}$	$^{85}\text{Kr}$	$^{222}\text{Rn}$
Activity concentration	1.8 Bq/m <sup>3</sup> Ar 1.7 Bq/m <sup>3</sup> air	1.2 MBq/m <sup>3</sup> Kr 1.4 Bq/m <sup>3</sup> air	5 Bq/m <sup>3</sup> air
Reference	[Loo 83]	[Bfs 01]	

The  $^{222}\text{Rn}$ -decay chain is more complex. In  $^{214}\text{Bi}$  and  $^{210}\text{Tl}$  decays,  $\gamma$  rays of more than 2 MeV energy are emitted. Monte-Carlo-simulations have shown [Bau 03] that a  $^{222}\text{Rn}$  activity of 0.5  $\mu\text{Bq}/\text{m}^3$  of nitrogen (STP) leads to a count rate of  $6 \cdot 10^{-5}$  cts/(keV $\cdot$ kg $\cdot$ y) in the energy window between 2 MeV and 2.08 MeV. Consequently nitrogen of this  $^{222}\text{Rn}$ -purity is sufficiently pure for the experiment.

Similar purity levels are required for liquid argon. When the scintillation of argon is exploited it might become necessary to remove  $^{85}\text{Kr}$  from the argon in order to reduce the overall count rate. The  $^{85}\text{Kr}$  activity should not exceed the  $^{39}\text{Ar}$  volumetric activity of 1.8 Bq/m<sup>3</sup> (STP). Therefore the volumetric krypton concentration in the argon has to be 1 ppm or lower.

### 5.8.1 Noble gas adsorption

Ultra pure gases are produced by adsorption of the impurities on dedicated adsorbers. For low partial pressures  $p$  the number of mols  $n$  of a gas that are adsorbed per mass of adsorber is given by Henrys law:  $n = H \cdot p$ ;  $H$  is the Henry constant. Since activated carbon usually has a wide pore size distribution, it is suited to trap different kind of impurities

independent of their molecular size. [Mau 00] gives the following empirical equation for the single component adsorption of un-polar gases on activated carbon:

$$H \left[ \frac{\text{mol}}{\text{kg} \cdot \text{Pa}} \right] = \exp \left\{ \left( -0,05 + \frac{81}{T[\text{K}]} \right) \cdot \frac{T_C[\text{K}]}{\sqrt{p_C[\text{bar}]}} - 17,5 \right\} \quad (10)$$

$T$  is the temperature and  $T_C$ ,  $p_C$  are the critical temperature and pressure of the adsorbed gas. Table 10 shows the critical parameters for the gases of interest and their calculated Henry constants for the adsorption on activated carbon at different temperatures.

Table 10: The critical pressures and temperatures for different gases and the calculated Henry constants for the adsorption on activated carbon.

Gas	$T_C$ [K]	$p_C$ [bar]	$T_C/\sqrt{p_C}$ [K/ $\sqrt{\text{bar}}$ ]	$H$ [mol/(kg·Pa)]			Ref.
				288 K	173 K	77 K	
Ar	150,7	48,6	21,6	$4 \cdot 10^{-6}$	$2 \cdot 10^{-4}$	63	[Atk 96]
N <sub>2</sub>	126,3	34,0	21,6	$4 \cdot 10^{-6}$	$2 \cdot 10^{-4}$	63	[Atk 96]
Kr	209,4	55,0	28,2	$2 \cdot 10^{-5}$	$3 \cdot 10^{-3}$	$5 \cdot 10^4$	[Atk 96]
Rn	377,0	62,8	47,6	$2 \cdot 10^{-3}$	10	$1 \cdot 10^{13}$	[Fle 03]

Being by far the heaviest gas of highest polarizability, radon can already be adsorbed efficiently at rather high temperatures (173 K). At liquid nitrogen temperature the Henry constant for radon becomes huge, so the radon is completely transferred from the gas phase to the adsorbed phase. Therefore no radon should remain in liquid nitrogen after running over an activated carbon column at 77 K. In practice re-contamination due to <sup>222</sup>Rn emanation of the activated carbon limits the obtainable purity. The BOREXINO collaboration uses the described technique to produce high purity nitrogen. The emanation problem could be solved by using a <sup>226</sup>Ra-free synthetic carbon (<sup>222</sup>Rn emanation rate ( $0.3 \pm 0.1$ ) mBq/kg [Heu 95]). In this case no radon was detected in the purified nitrogen. The obtained upper limit is  $0.3 \mu\text{Bq}/\text{m}^3$  (STP) [MPI 03].

The elimination of krypton is more difficult. Due to the similar adsorption properties of krypton and nitrogen/argon (see Table 10) a single component adsorption model fails to predict the equilibrium. The situation can be improved substantially if the adsorption happens in the gas phase at temperatures slightly above the boiling point of the gas to be purified. Further improvement is possible if carbon adsorbents with optimized pore size distributions are used. Doing so it is possible to achieve Henry constants for krypton of the order of 1 mol/(kg·Pa) at 95 K in the binary system krypton/nitrogen, and to purify more than 500 m<sup>3</sup> of nitrogen (STP) from krypton with only 1 kg of adsorber.

For argon the ratio of  $T_C$  and  $\sqrt{p_C}$  is the same as for nitrogen. Therefore the purification of argon from radon and krypton can be performed in the same way as the nitrogen purification. If the argon is to be instrumented, residual oxygen is of concern as it can quench the scintillation efficiency. The ICARUS collaboration has successfully operated a commercially available oxygen purification unit with liquid argon [Cen 93]. However, it is known that this material emanates radon. If such a device is implemented, it has to be located up-stream of the carbon adsorber to remove the emanated radon. In any case, the radon levels of the various components will be assayed prior to the finalization of the design.

The purification of nitrogen from argon is impossible by adsorption, because their adsorption properties are almost identical (see Table 10). A separation can only be achieved by rectification as it is done during the production of nitrogen in air separation plants. The BOREXINO collaboration has investigated high purity nitrogen from different suppliers [Zuz 04]. The best quality, see Table 11, has a volumetric argon concentration of 0.5 ppb, and is pure enough for the experiment. Moreover the volumetric krypton concentration

Table 11: Contaminations in commercially available liquid nitrogen.

Company	Ar [ppm]	Kr [ppt]	$^{222}\text{Rn}$ [ $\mu\text{Bq}/\text{m}^3$ ]
Air Liquide (4.0)	10	40	$\sim 50$
Linde (7.0)	0.06	0.3	?
SOL (6.0)	0.005	0.04	?
Westfalen AG (6.0)	0.0005	0.06	?

was 0.06 ppt. Therefore, it might not be necessary to build purification plants for krypton and argon. Radon, however, has to be removed before the detector is filled because it is emanated from most surfaces so a re-contamination can not be excluded. Since both LN and LAr are produced by the same process, rectification, one might expect that the krypton contamination of commercially available Ar 6.0 is less than 1 ppm, a value which should be verified by measurement, however.

### 5.8.2 Monitoring of liquid gas purity

Techniques to determine the amount of radon, krypton and argon in nitrogen have been developed for the BOREXINO experiment.  $^{222}\text{Rn}$  in nitrogen can be measured at the sub- $\mu\text{Bq}$ -level with proportional counters [Heu 95]. Argon and krypton concentrations are determined with a specially tuned rare gas mass spectrometer. The detection limits for 1 ccm nitrogen samples are  $\sim 1$  ppb for argon and  $\sim 0.1$  ppt for krypton [Zuz 04].

The detection of radon in argon can be done in the same way as described in [Heu 95], replacing nitrogen by argon. The radon from several  $100 \text{ m}^3$  of argon will be trapped on an activated carbon column cooled at liquid argon temperature. After removing most of

the argon the radon is filled into the proportional counter. To determine the krypton concentration in argon an extension of the technique applied for the determination of krypton in nitrogen is required, since mass spectrometers cannot handle macroscopic amounts of noble gases. It has been shown [Sim 03] that gas chromatography allows one to remove the largest fraction of argon, while at the same time the traces of krypton can be separated without loss [Sim 03]. The extracted krypton can then be measured with a standard mass spectrometer.

## 5.9 Water purification

The water shield will serve also as Cherenkov medium for the detection of incident muons. Purification of the water is necessary in order to keep the light transmissivity as high as possible. Origins of turbidity are dust and metal ions as well as biological activity from bacteria, for example. Contaminations from radioactive materials like Rn, Ra and Th should be less than the steel activity of 7 mBq/kg.

Water purification systems are essential for water Cherenkov detectors like Super-Kamiokande [SuK 03], Auger [Aug 97] or the BOREXINO counting test facility (CTF) [Ali 98] where the design goal for the radiopurity of the water shield is  $10^{-6}$  Bq/kg. The radon content of the LNGS water is  $10^4$  Bq/m<sup>3</sup>.

The purification systems consist in general of several components including  $\mu$ m absolute filters, ion exchangers for the removal of metal ions, ultra violet sterilizers to kill bacteria, and ultra filters to remove nanometer sized particles [Aug 97, Ali 98, SuK 03]. The purity of the water is monitored by measuring in particular its resistivity which reaches after the ultra filter the chemical limit of 18 M $\Omega$ .cm [SuK 03]. Radon may be removed either by a vacuum de-gasifier [SuK 03] or by a counter-flow of nitrogen like in the BOREXINO CTF [Ali 98].

The capacity of the BOREXINO CTF purification system is designed for 1000 tons of water. In order to save cost and space, we propose to use this system for producing the  $\sim$ 500 tons of water needed for the planned experiment. In view of the sealed and rust-protected water container, a small and dedicated continuous re-circulation system with a sub-micron filter and an ultra violet sterilizer will be sufficient to maintain the water quality.

## 5.10 Liquid gas storage

Storage tanks are needed to provide timely the LN (or LAr) lost by evaporation. This loss will range - dependent on vessel volume and type of insulation - from 0.1 to 1 m<sup>3</sup> per day. Hermetic storage of freshly delivered liquid gas over a few weeks is also a cheap yet efficient method to reduce the content of radon by profiting from its half-life of less than 4 days.

Close to Hall A two storage tanks are located with a capacity of 5 m<sup>3</sup> each. So far, they have been used by the GNO experiment. These tanks might be suitable for the planned experiment and we propose to allocate them to it. However, their compatibility with the required low Ar, Kr and Rn concentrations has to be checked.



## 6 Procurement of enriched $^{76}\text{Ge}$ detectors

### 6.1 Modification of existing $^{76}\text{Ge}$ detectors

There are available five, respectively three, enriched  $^{76}\text{Ge}$  detectors from the Heidelberg-Moscow (HdM) and IGEX collaboration with a mass of about 2 kg each. All these detectors are of p-type and manufactured in a similar way. At present, these detectors are still housed in cryostats stored underground either at LNGS, Canfranc or Baksan. For the use in the proposed experiment, it is necessary to take these detectors out of their cryostats (see Fig. 18, left side) and to remove the old contacts. After a cleaning procedure the detectors need to be equipped with new contacts. Two possible solutions are depicted in the middle

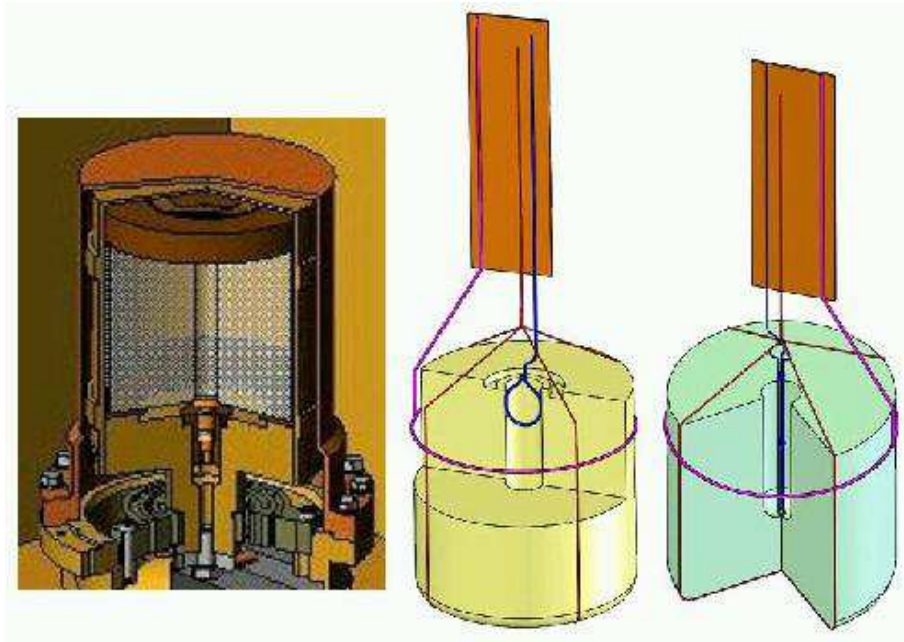


Figure 18: The conventional way of a Ge-diode mount (left) and proposed suspension and contacts for IGEX type (middle) and HdM-type (right) enriched  $^{76}\text{Ge}$  diodes.

and right part of Fig. 18. For the IGEX type diodes, a steel spring wire of 0.5 mm diameter serves as inner signal contact. The suspension strings as well as the HV contact are fixed by the same material which - by use of a tiny spanner nut - is tightly laid around the outer surface of the Ge cylinder. As to the inner contact of the HdM-type diodes, three legs of the steel spring wire are welded together and bound on top in such a way that they form a spring; attached at the merging point of the suspension strings, the spring load presses the tip against the core bottom. This contact could also be installed upside down. Another alternative would be a hollow stem made of electro-formed Cu with a spring coil on top. At the crystal interface the contacts will be gold plated. However, the optimal low-mass

contact solution would be to bond the wires directly to the crystal surface, and tests are in progress.

The suspension strings consist of 0.5 mm Dyneema fiber. While the figure shows four legs, three should be sufficient. Both contacts and the central suspension are integrated into a Kapton strip to assure fixed spacing (capacity) between the wires.

The approximate weight of the materials close to the crystal hardly exceeds 2.6 g (spring wire  $\sim$ 0.4 g, fiber  $\sim$ 0.2 g, screw system close to 2 g). This compares with a mass of 3.5 kg for the HdM detectors which is mainly due to the copper envelope and cap. The total surface area of the described solution is about 200 times smaller than in the conventional case. All materials to be used have been checked already by Ge screening at Heidelberg to be radiopure below a level of a few 10 mBq/kg. Measurements with higher sensitivity are planned. Mechanical stability tests of these materials at liquid nitrogen temperature have been performed with satisfying results.

Any effort will be made that all modifications are done underground in order to avoid a new contamination of the crystals by cosmogenic radioactivity.

## 6.2 Fabrication of enriched $^{76}\text{Ge}$ detectors

The fabrication of intrinsic Ge detectors is usually the realm of commercial companies. With respect to enriched detectors, however, several problems have to be overcome. One problem is the procurement of enriched material which - at affordable cost - can only be supplied by Russian companies; another problem is the cosmogenic radioactive contamination of the  $^{76}\text{Ge}$  material if it is kept at sea level and not stored immediately underground (see chapter 'Background simulations').

### 6.2.1 Procurement of enriched $^{76}\text{Ge}$

Information from the Ministry of Atomic Energy of Russia obtained by the end of 2003 and in January 2004 indicate that enriched Ge can be acquired from the Svetlana plant which is a special department of the Zelenogorsk electro-chemical plant (ECP). Together with the Kurchatov institute ECP has already supplied the enriched material for the Heidelberg-Moscow and IGEX experiments. The separation is done in centrifuges for stable isotopes. The necessary natural Ge has to be supplied by the customer (14 kg for 1 kg of 85% enriched  $^{76}\text{Ge}$ ). The preferred form of natural Ge is metal granulate but metal bars are also accepted. Its purity should be  $>99\%$ . Typical and easily available qualities are 4N or 5N. The enriched Ge will be delivered as  $\text{GeO}_2$ ; at slightly higher cost, however, delivery as metal is also possible. For each batch the contaminations will be specified. The Ge waste material can be returned on customer's request either as  $\text{GeO}_2$  or Ge metal.

The minimum batch is 30 kg of enriched  $^{76}\text{Ge}$ . At the beginning, however, a test run yielding about 2 to 4 kg enriched  $^{76}\text{Ge}$  for material validation is possible. The maximum production capacity is 200 kg per year, and the enrichment process will run without any interruption. The price is 45 to 50 US\$ per gram 85% enriched  $^{76}\text{Ge}$  plus the cost of the natural germanium.

Research at the Institute of Molecular Physics of the RCC Kurchatov is pursuing an alternative separation process based on  $\text{GeCl}_4$ . Thus expensive chemistry steps for the conversion of germanium into  $\text{GeF}_4$  could be reduced resulting in a presumably lower price for the enriched material (see section 7.6).

### 6.2.2 Processing of $^{76}\text{GeO}_2$ to intrinsic $^{76}\text{Ge}$ crystals

In Europe, we know of only one big commercial company which does both the reduction of  $\text{GeO}_2$  to metal, the subsequent zone refining to the level of a few  $10^{10}$  impurities per  $\text{cm}^3$  required for the production of intrinsic Ge diodes, as well as the crystal pulling. Different from the past, the reduction is no longer done in a wet chemistry environment but in a hot  $\text{H}_2$  atmosphere which leads us to expect that the losses of enriched material become negligible in this step. The processing of Ge material is carried out on large scale and it has to be explored how the separate processing of relatively small amounts of enriched  $^{76}\text{Ge}$  material would fit into the production flow. First encouraging contacts have been made.

### 6.2.3 Detector fabrication

There is no evidence that fabrication of intrinsic Ge detectors is made more difficult if isotopically shifted material is used. The enriched  $^{76}\text{Ge}$  detectors of the Heidelberg-Moscow and IGEX experiments, more than 10 detectors with an active mass of about 20 kg, have been manufactured by commercial companies and operated subsequently for more than 80 kg.years.

Natural Ge (p-type) detectors which have proven to operate in LN or LAr have been supplied by three companies so far, and we see no reason that this success is due to any proprietary technique.

Table 12: Estimated time which has to be allocated to various detector processing steps.

Step	time needed
polyzone refining	2 days
mono-zone refinement incl. quality control meas.	7-8 days
crystal pulling incl. last zone refining	2 days
production of standard 2kg Ge diode	approx. 2 weeks

The major constraint for the fabrication of  $^{76}\text{Ge}$  detectors for  $0\nu\beta\beta$  decay experiments comes from the fact that - without prevention - at sea level cosmic radiation produces various radioactive isotopes of which  $^{60}\text{Co}$  is most detrimental due to its long half life of 5.3 years. Being a contaminant in Ge,  $^{60}\text{Co}$  is still removable by zone refining, and thus the clock for its production starts to tick at the end of the last zone refining step. Table 12 shows the time needed by a big supplier for the different processing steps from zone refining to the detector end product. For optimum conditions, this implies that detector

production, at least, must be done underground. Until such a facility is available, it might be possible to select suppliers which can store the crystals underground in the periods where the manufacturing process is interrupted.

#### **6.2.4 Loss of $^{76}\text{Ge}$ material during processing**

The IGEX collaboration has lost about 5% of enriched  $^{76}\text{Ge}$  material during the various steps of processing [Maj 03] and is aiming now at less than 3%. At present, we are not able to provide a reliable estimate.

## 7 R&D program

The schedule for the R&D projects reflects the different phases of the experiment: there will be a relatively short phase of R&D aiming at optimizing the experimental setup and the performance of the existing enriched detectors in experiment, followed by a second intermediate phase which focuses on the optimum design for the new enriched detectors, on their fabrication and a further enhancement of the performance of the whole setup including the instrumentation of the liquid argon. Nevertheless, much work for the intermediate term R&D will be done in parallel with the short term activity and will start immediately.

### 7.1 Mechanical engineering

A short term project is the design of the interlock system between the vessel and the outside world. This system is closely connected with the suspension system for up to 50 natural and enriched Ge diodes. An important requirement is the possibility to exchange a small part of the diodes without removal of the whole detector array from the vessel. The suspension system has to solve contradicting requirements: while mass reduction is the first goal, it, nevertheless, must be rigid and guarantee a well defined orientation and location of the diodes. This task is becoming even more difficult in view of the constraint that only materials of established radiopurity are allowed for construction.

Further short term mechanical R&D has to address the design of a system which allows to introduce temporarily radioactive sources into the vessel for periodically establishing the energy calibration of the Ge diodes. The system must allow one to position these sources at various precisely known locations so that all detectors are well 'illuminated' and the resulting spectra can be used in the comparison with the Monte Carlo simulations of the detector array. Obviously, also this project is closely linked to the interlock and suspension system. Possible solutions are permanently installed plastic tubes through which the sources are inserted and removed, or an internal manipulator system whose remotely controlled arms move the sources from their shielded location to the detectors and back.

### 7.2 Electronic engineering

Stable yet ultra-low mass contacts at the crystal are the prerequisite for a reliable low-noise operation of the diode. The optimum solution might be ultrasonic bonding with aluminum or gold wires of typically 20  $\mu\text{m}$  diameter. This method is also used for contacting segmented Ge detectors, and first tests with a dummy Ge crystal have yielded encouraging results. The end of the delicate bond wire would be attached to the signal or high voltage cable which must, however, be fixed with respect to the crystal in order to avoid stress onto the delicate bond wire.

The readout cable should be flexible, even at LN temperature, hold high voltages up to 4 or 5 kV, exhibit a low impedance for maintaining the pulse characteristics in the time domain, and be well shielded to minimize cross talk; in addition it should consist

of radiopure materials only. First tests showed that Kapton cables with copper traces represent a promising candidate. More work has to be done to come up with an optimum solution.

In cryostat-housed Ge detectors, the FET of the preamplifier stage is usually mounted close to the diode on the cool finger. A little piece of plastic between cool finger and FET serves as thermal impedance and makes the FET run at about 20°C above the LN temperature at optimum noise performance. This approach is presumably not possible in LN, and it has to be investigated if there are commercial FETs available which are suited to run at LN temperature, or a dedicated FET has to be designed which does not exhibit carrier freeze out. Since the cable between FET and preamplifier might be still several meters long, the most straightforward way to best performance will be to put not only the FET but the whole preamplifier close to the diode, which - on a few mm<sup>2</sup> large silicon die - can be realized by a fully integrated VLSI solution. The AGATA collaboration has reported encouraging progress in this field, and R&D on such a device can be done at the Heidelberg ASIC laboratory where the MPI Heidelberg has developed already a VLSI readout ASIC for silicon strip detectors.

### 7.3 Monte Carlo simulations

An urgent topic is the simulation of the planned final vessel setup in order to arrive at a full understanding of its shielding power, and to optimize the use of shielding materials. Monte-Carlo simulations will be used also for the layout of the muon shield including the water Cherenkov detector.

As soon as the vessel layout is fixed, a detailed Monte Carlo description of the experimental setup has to be developed including the database which documents the evolution of the experimental setup with time.

Obviously, the present simulations have focused on the most important backgrounds in the 2 MeV region only. However, it is desirable to study also rare processes in order to deepen the quantitative understanding of the observed background at all energies. This will be of prime importance for dark matter studies for which the low energy part of the measured spectrum has to be understood quantitatively.

### 7.4 Validation of materials

Screening of materials to be used for shielding, support and contacts of the Ge diodes is of utmost importance. So far, these investigations have profited very much from the most sensitive GeMPI setup at LNGS. Present measurements include the determination of the radioactivity of several samples of commercially available lead which could be used for the vessel shielding. The assembly of a similar second station is in progress. In addition, with the termination of the LENS prototype phase, the "Low background LENS facility" might be used as powerful large volume screening device.

Low background measurement devices of a different setup, exhibiting e.g. multi detector arrays, are installed at the Baksan underground laboratory and use of these facilities will

be possible by the Russian signers of this Letter of Intent.

## 7.5 Detector R&D

Basic detector R&D will start with a simulation of the field distribution in various variants of p-type Ge diodes which will eventually result in an optimized design of the detectors as well as in a better understanding of the pulse shapes expected for single- and multi-site events.

R&D with commercial suppliers of Ge diodes will focus on the efficient manufacturing of axially segmented p-type detectors. These devices are easier to build than n-type diodes, and their robust outside dead-layer does both ease the handling and provide an integrated shield against  $\alpha$  particles which outweighs the loss of sensitive volume. Tests with radioactive sources will establish how much information can reliably be extracted from pulse shapes, and how well internal background processes can be suppressed by the anti-coincidence between different segments. This experimental program will be accompanied by Monte Carlo simulations.

As outlined at several occasions above, the fabrication of new enriched Ge diodes should be done preferentially underground. This way, not only cosmogenic contaminations can be minimized but complete control of the cleanliness of the production cycle becomes possible, too. In addition, as known from estimates within the AGATA collaboration, our own production might be more cost-effective than ordering from a commercial supplier. A realization of this plan would imply a long term engagement and needs to be prepared with a most detailed R&D plan. At present, it is premature to outline such a plan. However, it is in this context interesting to know that similar considerations exist within the AGATA collaboration, and a merge of the interested parties might turn out to be beneficial for both sides with respect to sharing of resources, know-how transfer and training for the fabrication of Ge diodes.

Eventually, an extension of Ge technology to thin and highly segmented Ge diodes might open a new and perhaps more powerful way for the suppression of both internal and external backgrounds.

## 7.6 Germanium enrichment

Currently the enrichment process is performed with gas centrifuges using  $\text{GeF}_4$ . While this is a well proven technology there are some disadvantages: the chemical treatment for  $\text{GeF}_4$  is relatively expensive and there could be contaminations from uranium since the  $\text{F}_2$  gas used is typically recycled from  $\text{UF}_6$  enrichments. This contamination will accumulate in the separation step for  $^{76}\text{Ge}$ .

Researchers at the Institute of Molecular Physics of the Kurchatov Institute have developed a new Ge isotope selection technique based on  $\text{GeCl}_4$ . This method has been established for the production of a few grams of  $^{76}\text{Ge}$ .  $\text{GeCl}_4$  is a commercially available compound with high chemical purity, and the disadvantages mentioned for  $\text{GeF}_4$  are avoided. The main limitation of this approach stems from the fact that chlorine has two

stable isotopes ( $^{35}\text{Cl}$  and  $^{37}\text{Cl}$ ) and the heavier one has only an abundance of 24%. The maximum possible enrichment fraction amounts to about 40%. For higher enrichments the  $\text{GeF}_4$  technology has to be used which would require in this case much less material and would be more efficient.

The extension of the  $\text{GeCl}_4$  technology to produce a few kg of enriched material is one of the foreseen R&D topics. Its isotope selection and economical efficiency will be studied in detail. In addition it is planned to develop measurement techniques to identify the U/Th contamination in the raw and enriched germanium material. Once established this will be applied for monitoring the separation process.

## 7.7 Instrumentation of liquid argon

Scintillation light in liquid argon is well established [Kub 79, Dok 90, Hit 83, Cen 99]. Its potential for internal and external background rejection can be realized only if the UV light is efficiently collected. Cosmic ray muons create large signals and thus can be vetoed readily. In order to achieve an efficient anti-coincidence shield for cosmogenic activities such as internal  $^{60}\text{Co}$  or  $^{68}\text{Ge}$ , or external gammas from  $^{208}\text{Tl}$ , an effective threshold of typically 100 keV should be achieved. An additional requirement is that materials for shifting and guiding the scintillation photons to the photo sensors, as well as the photo sensors themselves must not augment the background signal in the germanium detectors. With instrumented LAr, a densely packed Ge diode array is not the optimum detector arrangement since the diodes are an obstacle for the light collection. The optimum geometry has to be resolved with Monte Carlo studies.

The scintillation yield of liquid argon is 40,000 photons per MeV and the wavelength of the emitted photons is 128 nm. The strategy to detect these photons is to shift them to a wavelength of about 400 nm and to transport them via specular reflection to photomultiplier tubes immersed in liquid argon. A transparent wavelength shifter developed for IceCUBE [Res 04] combined with an efficient reflector foil [Mot 04] appear as an attractive solution. First experimental tests have started using a PMT (ETL 9367 KFLB) immersed in liquid argon combined with wavelength shifting and reflector foils. Fig. 19 shows the recorded pulse shape for muons. Next steps in the R&D programme comprise the operation of a germanium crystal in anti-coincidence with the liquid argon scintillation and measurements of photo-electron yields for different wavelength shifting materials.





Figure 19: Measured response to a muon crossing the LAr volume with the characteristic fast and slow pulse component.

## 8 Safety

The present status of the proposed experiment does not yet allow a detailed safety discussion. On the other hand, the major generic safety aspects are known, and this chapter serves to discuss them and to prove that safety aspects are observed already in the early planning stage of the experiment.

Tables 13 and 14 identify potential hazards which may be caused by the installation of the proposed experiment. The still incomplete tables follow the initial safety informa-

Table 13: Initial safety information for the proposed experiment, excluding the construction phase.

SPOKESPERSON:..... tbd		GLIMOS:..... tbd		
(1) GASES, LIQUIDS, CRYOFLUIDS (used in detectors or kept nearby)				
Device Type	Fluid	Volume	Abs. Press.	Max Flow
> Exp. tank	LN or LAr	<400 m <sup>3</sup>	1.2 atm	
> Exp. tank	water	<500 m <sup>3</sup>	1.0 atm	
(2) OTHER CHEMICALS				
(Toxic/Corrosive/Flammable solvents, additives etc):				
> depending on type, vessel isolation may emit toxic gases if burning				
> small amounts of cleaning fluids like alcohol				
(3) ELECTRICITY				
MAGNETS: > NONE				
High Voltage (>1 kV)				
Detector Type	Voltage	Current	Stored Energy	No of HV channels
> Ge diode	<5 kV	<1 nA		<50
> PM	<3 kV	<3 mA		$\mathcal{O}(100)$
SHORT-CIRCUIT current >5 mA for >50V possible anywhere? > (NO)				
POWER dissipated by all electronics				
a) on detectors: > negligible    b) off detectors: > to be specified				
SPECIAL GROUNDING REQUIREMENTS? > NONE				

tion requested for experiments at CERN [Ced 72]. Information on the spokesperson and the group leader in matter of safety (GLIMOS) is not yet available. Table 13 shows that an impact on the environment by toxic or corrosive materials is excluded. No flammable gases and liquids are used. However, certain types of insulation under consideration (e.g. polyurethane) do emit toxic gases if they are burning. Replacements are under investigation. The radioactive sources needed for the energy calibration of the Ge detectors will be all encapsulated, and their activity will be low enough so that no regulations beyond the standard radiation protection rules are needed.

Table 14: Initial safety information for the proposed experiment, excluding the construction phase (continued).

<b>(4) LIFTING AND HANDLING</b>			
Weight of heaviest single piece to install?	> to be specified		
Specially designed handling equipment?	For which max. weight?		
<b>(5) VACUUM TANK, PRESSURE TANK, CRYO-TANK</b>			
Tank	Abs. pressure	Volume	Weakest part of wall
> Cryo-tank (exp.)	1.2 atm.	<250 m <sup>3</sup>	
> Cryo-tank1 (storage)	to be specified		
> Cryo-tank2 (storage)	to be specified		
<b>(6) IONIZING RADIATION (radioact. sources, depleted uranium, etc.)</b>			
Radioactive source	> for calibration, to be specified		
<b>(7) NON-IONIZING RADIATION (Laser, UV light, microwaves, rf)</b>			
> UV laser for PMT calibration			
> possibly UV light for sterilizing water			
<b>(8) OTHER HAZARDS</b>			
> suffocation			
> electric shorts induced by water leak			
<b>(9) RISK ANALYSIS</b>			
> to be done for big LN/LAr/water vessel			

The major potential hazard is due to the big cryostat of the experiment which will contain a maximum of 250 m<sup>3</sup> of liquid nitrogen (LN) or liquid argon (LAr). Table 15 gives a compilation of the physical properties of these cryogenic liquids [TIS 09].

The amount of stored LN or LAr corresponds to a gaseous volume of about 210000 (180000) m<sup>3</sup>; this is about 9 (7) times the volume of Hall A. The specified daily evaporation is less than 0.5% of the liquid, or less than 10% of the volume of Hall A. At standard operation, the present ventilation system guarantees that 40% of the air is exchanged per hour in each of the three halls, or an ‘air-washing’ of the total volume of each hall within 2.5 hours.

Argon and nitrogen are inert, non-toxic and non-flammable gases. However, if they replace part of the oxygen in the atmosphere, severe damage to human beings can result. This hazard is increased in a confined space like an underground hall with limited ventilation. Thus, as a result of leakage, the hazards will be essentially that of asphyxiation and injuries due to the low temperature - frostbites, cryo-burns, hypothermia and others. Similarly, due to low temperature further damage could result to structures and equipment impinged on by the cryofluid. A risk analysis has to show which measures are needed to prevent a major accident, and to minimize the risks and effects of a major accident. On

Table 15: Physical properties of liquid nitrogen and argon

Characteristics	Argon	Nitrogen	Unit
Boiling point at 1 bar	-185.5	-195.8	°C
	87.3	77.3	K
Density of liquid at boiling point	1400	810	kg/m <sup>3</sup>
Liters of gas at 20°C produced by 1 liter of liquid, 1 bar	841	693	liters
Density at 20°C compared to density of air	1.4	1.0	
Latent heat of evaporation for 1 liter of liquid	220	160	kJ
Ratio of enthalpy of vapor at 20°C and latent heat of evaporation	0.7	1.14	

the other hand, it is known [Ful 88] that the use of a doubly-walled cryogenic vessel with passive insulation makes it highly unlikely that a major leakage of liquid fluid can develop. A study of a super-insulated vessel version has shown that the requirement to withstand a standard earthquake can be met rather easily [Bab 03].

All other potential hazards are not aggravated due to the fact that the experiment will be operated underground. It is intended to plan and to build the experiment and its infrastructure following the ‘Safety Guide of the LNGs’ and the safety rules of CERN. In particular, it is intended to provide in due time documentation of the safety relevant components.

This documentation will include

- tank cooling down and filling procedure,
- tank emptying procedure,
- description/location of relieve and safety valves,
- description/location of temperature and pressure sensors,
- description/location of gas collector diffusers,
- description/location of oxygen monitors,
- description of gas control system and its operation,
- inventory of installed electrical cables,
- description of fire extinguishing system
- risk analysis/matrix with respect to LN/LAr/water leakage,
- risk analysis/matrix considering earthquake, statics calculations
- risk analysis/matrix considering power black-out,
- risk analysis/matrix considering possibility of burning insulation.

The overall safety of the experiment will profit from a fully computerized control and monitoring system with remote access that will record all safety relevant parameters. The

critical parts of this highly reliable and redundant detector safety system will be based on an autonomously running programmable logic controller (PLC) front-end. In case of any alarm condition, the data will be communicated to the LNGS general safety monitoring system which will trigger the necessary action and contact the experiment's on-call duty. In case of electrical power outage, a UPS module makes it possible to continue data taking or to automatically bring all critical system components into a safe state.

## 9 Time schedule

The experiment is divided into two phases as shown in Table 16. A third phase is considered. Phase I starts with the construction of the experimental facility, and measurements

Table 16: Phases of the planned experiment

	2005	2006	2007	2008	2009	2010
<b>Phase I</b>						
Construction	■					
Measurement with existing $^{76}\text{Ge}$ diodes		■	■	■	■	■
<b>Phase II</b>						
Procurement of enriched $^{76}\text{Ge}$ material	■	■				
Production of new $^{76}\text{Ge}$ diodes		■	■			
Measurement with all $^{76}\text{Ge}$ diodes			■	■	■	■

begin one year later using both natural Ge diodes as well as the major part of the existing almost 20 kg enriched  $^{76}\text{Ge}$  diodes. The actual beginning of Phase II is determined by the availability of funds for the procurement of enriched  $^{76}\text{Ge}$  material and the fabrication of new probably segmented enriched  $^{76}\text{Ge}$  detectors. We assume this is the case soon after the construction is finished. With the new detectors the running will continue until about hundred (kg·years) have been accumulated and backgrounds start to show up. The outcome of this Phase II will determine how Phase III has to be defined.

Table 17 shows in more detail the schedule for the construction period in Phase I. It is assumed that the funds are secured by the end of the third quarter in 2004. The procurement time for the vessel accounts for the need to have an European-wide call for tenders. The first steps towards the procurement of enriched  $^{76}\text{Ge}$  material will be made as soon as funds are available in order to avoid any loss in time.

Table 17: Proposed technical time schedule for Phase I

	2004				2005			
	Q1	Q2	Q3	Q4	Q1	Q2	Q3	Q4
<b>LoI</b>	██████████							
<b>Proposal</b>			██████████					
<b>Tank</b>								
Review, optimize		██████████						
Procure				██████████				
Construct					██████████			
Install							██████████	
Cryogenic commissioning								██████████
<b>Lock, suspension, calibration</b>								
Design		██████████						
Fabricate, test					██████████			
Install							██████████	
<b>Muon veto system</b>								
Design/build				██████████				
Install								██████████
<b>Electronics</b>								
Frontend R&D		██████████						
Optimize contacts, cables		██████████						
Design/build frontend				██████████				
Design DAQ/database			██████████		██████████			
Install/test DAQ					██████████			
<b>Ge diodes</b>								
Modify existing diodes			██████████					
Test modified diodes					██████████			
Simulate segmented diodes			██████████					
Procure segmented diode					██████████			
Test diodes in LN and LAr	██████████				██████████			
Install diodes								██████████
<b>Enriched <sup>76</sup>Ge detectors</b>								
Procure test batch material				██████████				
Validate material					██████████			
Build/test small test diode					██████████			
Order more enriched material							██████████	

## References

- [Aal 99] C.E. Aalseth et al., Phys. Rev. C59 (1999) 2108.
- [AGA] “Advanced GAMMA Tracking Array” (AGATA) project, <http://agata.pd.infn.it/index.html>, and [npg.dl.ac.uk/AGATA/](http://npg.dl.ac.uk/AGATA/)
- [Ali 98] G. Alimonti *et al.*, Nucl. Instr. Meth. A406 (1998) 411-426.
- [Ali 98b] G. Alimonti *et al.*, Astr. Part. Phys. 8 (1998) 141.
- [All 03] S.W. Allen, R.W. Schmidt and S.L. Bridle, Mon. Not. Roy. Astron. Soc. 346 (2003) 593, and astro-ph/0306386.
- [Arn 03] C. Arnaboldi *et al.*, (CUORE collaboration), Astropart. Phys. 20 (2003) 91.
- [Arn 04] C. Arnaboldi *et al.*, Phys. Lett. B584 (2004) 260-268.
- [Arno04] R. Arnold *et al.*, preprint submitted to Nucl. Instr. Meth. A, physics/0402115.
- [Arp 92] C.Arpesella, Nucl. Phys. B (Proc. Suppl.) 28A (1992) 420.
- [Ash 03] V.D.Ashithov *et al.*, nucl-ex/0309001.
- [Atk 96] P.W. Atkins, *Physikalische Chemie* (1996) VCH Verlagsgesellschaft mbH, Weinheim.
- [Aug 97] Pierre Auger Project Design Report (1997) <http://www.auger.org/admin/DesignReport>
- [Aug 03] C. Augier, International Workshop on Weak Interactions in Nuclei and Astrophysics: Standard Model and Beyond ECT, Trento, 16 - 21 June (2003)
- [Avi 92] F.T.Avignone *et al.*, Nucl. Phys. B (Proc. Suppl.) 28A, (1992) 280.
- [Bab 03] Babcock Noell Nuclear GmbH, ‘*Preliminary study on the feasibility of a liquid nitrogen vessel*’ (2003) BNN-Order No S.919005.
- [Bak 03] A.M. Bakalyarov *et al.*, hep-ex/0309016.
- [Bar 02] A.S. Barabash, Proc. Int. Workshop on technique and application of xenon detectors, Edts. Y. Suzuki, M. Nakahata, Y. Koshio and S. Moriyama, Univ. of Tokyo, Japan Dec. 2001, World Scientific, (2002) p. 101-114.
- [Bau 99] L. Baudis, ‘*Suche nach dem neutrinolosen Doppelbetazerfall und nach dunkler Materie mit HPGe-Detektoren*’, Dissertation (1999), Universität Heidelberg.
- [Bau 03] L. Baudis *et al.*, Nucl. Instr. Meth. A481 (2002) 149-159.



- [Bel 01] G. Bellini *et al.*, Eur. Phys. J. C19 (2001) 43.
- [Bfs 01] Bundesamt für Strahlenschutz (BfS), ‘*Künstliche Umweltradioaktivität*’ Jahresbericht (2001) 63.
- [Ced 72] CERN EDMS # 383772
- [Cen 93] P. Cennini *et al.*, Nucl. Instr. Meth. A333 (1993) 567-570.
- [Cen 99] P. Cennini *et al.*, Nucl. Instr. Meth. A432 (1999) 240-248.
- [Cmp 04] CMP Arles, dept. cryogénie Soisson, 02201 Soisson, France.
- [Dan 00] F.A. Danevich *et al.*, Phys. Rev. C62 (2000) 044501.
- [Del 03] <http://www-dapnia.cea.fr/Sphn/Deformes/Agata/preamps/index.shtml>
- [Die 99] A. Dietz, Diplomarbeit (1999), Universität Heidelberg.
- [Dör 03] Ch. Dörr, H.V. Klapdor-Kleingrothaus, Nucl. Instr. Meth. A 513 (2003) 596-621, and Ch. Dörr, Diplomarbeit (2002), Universität Heidelberg.
- [Dok 90] T. Doke *et al.*, Nucl. Instr. Meth. A291 (1990) 617.
- [Eji 00] H. Ejiri *et al.*, Phys. Rev. Lett. 85 (2000) 2917.
- [Elg 03] Ø. Elgarøy, O. Lahav, JCAP 0304 (2003) 004.
- [Ell 02] S.R. Elliott and P. Vogel, Ann. Rev. Nucl. Part. Sci. 52 (2002) 115-151.
- [Fer 03] F. Feruglio *et al.*, Nucl. Phys. B659 (2003) 359-362.
- [Fle 03] Flexware Inc., <http://www.flexwareinc.com/gasprop.htm> .
- [Ful 88] N.J. Fulford and M.D. Slatter, Cryogenics 28 (1988) 810-817.
- [Giu 03] A. Giuliani, TAUP 2003 conf. proceedings., Nucl. Phys. B (Proc. Suppl.), in press.
- [Heu 95] G. Heusser, Ann. Rev. Nucl. Part. Sci. 45 (1995) 543.
- [Heu 00] G. Heusser *et al.*, Appl. Rad. and Isot. 52 (2000) 691-695.
- [Hit 83] A. Hitachi *et al.*, Phys. Rev. B 27 (1983) 5279.
- [JLG 04] JL Goslar GmbH, ‘*Untersuchung über den Bau eines Bleiabschirmtanks*’ (2004).
- [Jor 94] V.T. Jordanov and G.F. Knoll, Nucl. Instr. Meth. A345 (1994) 337-345.

- [Jor 03] V.T. Jordanov, Nucl. Instr. Meth. A505 (2003) 347-351.
- [Kih 03] T. Kihm, V.F. Bobrakov, H.V. Klapdor-Kleingrothaus, Nucl. Instr. Meth. A498 (2003) 334-339.
- [Kla 99] H.V. Klapdor-Kleingrothaus *et al.*, MPI-Report MPI-H-V26-1999, and hep-ph/9910205, and L. Baudis *et al.*, Nucl. Instr. Meth. A426 (1999) 425-435.
- [Kla 01] H.V. Klapdor-Kleingrothaus *et al.*, Eur. Phys. J. A12 (2001) 147.
- [Kla 03] H.V. Klapdor-Kleingrothaus *et al.*, Nucl. Instr. Meth. A510 (2003) 281-289.
- [Kla 03a] H.V. Klapdor-Kleingrothaus *et al.*, Nucl. Instr. Meth. A511 (2003) 341-346.
- [Kla 04] H.V. Klapdor-Kleingrothaus *et al.*, ‘*Data acquisition and analysis of the  $^{76}\text{Ge}$  double beta experiment in Gran Sasso 1990-2003*’, Nucl. Instr. Meth. A, in press, doi:10.1016/j.nima.2003.12.013.
- [Kub 79] S. Kubota *et al.*, Phys. Rev. B20 (1979) 3486.
- [Laz 03] L.H. Lazarus, preprint 2003, <http://nnsa.dl.ac.uk/GRT/>
- [Loo 83] H.H. Loosli, Earth and Planetary Sci. Lett. 63 (1983) 51-62.
- [Mai 96] B. Maier, Dissertation (1996), Universität Heidelberg; and J. Bockholt, Dissertation (1994), Universität Heidelberg.
- [Maj 03] White Paper on the Majorana Zero-Neutrino Double-Beta Decay Experiment, MAJORANA collaboration (2003), nucl-ex/0311013.
- [Mau 00] S. Maurer: ‘*Prediction of Single-Component Adsorption Equilibria*’, Dissertation, Technische University München, Herbert Utz Verlag – Wissenschaft (2000).
- [Mot 04] D. Motta, Dissertation, Universität Heidelberg, in preparation
- [MPI 03] Max-Planck-Institut für Kernphysik, *Progress Report* (2003), Heidelberg.
- [Ned 00] H. Neder, G. Heusser and M. Laubenstein, Appl. Rad. Isot. 53 (2000) 191-195.
- [Osi 01] A. Osipowicz *et al.* (KATRIN collaboration), hep-ex/0109033.
- [Pan 04] L. Pandola *et al.*, ‘*Neural network pulse shape analysis for proportional counter events*’, Nucl. Instr. Meth. A, in press.
- [Res 04] E. Resconi and S. Schönert, to be submitted to Nucl. Instr. Meth. .
- [Sho 99] A.L. Shoup (Milagro collaboration), astro-ph/9907214.

- [Sim 03] H. Simgen, '*Hochempfindlicher Nachweis radioaktiver Edelgasnuklide und natürlicher Radionuklide aus der Uran-Zerfallsreihe*', Dissertation (2003), Universität Heidelberg, <http://www.ub.uni-heidelberg.de/archiv/3731>
- [Spe 03] D.N. Spergel *et al.*, *ApJ Suppl.* 148 (2003) 175.
- [SuK 03] The Super-Kamiokande Collaboration, *Nucl. Instr. Meth.* A501 (2003) 418-462.
- [TIS 09] '*The use of cryogenic fluids*', (1998) CERN TIS IS 47.
- [Wul 03] H.R.T. Wulandari, '*Study on Neutron-Induced Background in the Dark Matter Experiment CRESST*', Dissertation (2003), Technische Universität München, and H.R.T. Wulandari *et al.*, hep-ex/0401032.
- [XIA] X-Ray Instrumentation Associates (XIA), <http://www.xia.com> .
- [Zde 01] Yu.G. Zdesenko, O.A. Ponkratenko, V.I. Tretyak, *J. Phys.* G27 (2001) 2129.
- [Zub 01] K. Zuber, *Phys. Lett. B* 519 (2001) 1.
- [Zuz 04] G. Zuzel *et al.*, '*Ar and Kr concentrations in nitrogen as a measure of the  $^{39}\text{Ar}$  and  $^{85}\text{Kr}$  activity in connection with the solar neutrino experiment BOREXINO*', *Appl. Rad. Isot.*, in press.